

Changes in urban heat island intensity with background temperature and humidity and their associations with near-surface thermodynamic processes

Kyeongjoo Park ^a, Jong-Jin Baik ^{a,*}, Han-Gyul Jin ^{b,c}, Abeda Tabassum ^a

^a School of Earth and Environmental Sciences, Seoul National University, Seoul 08826, South Korea

^b Department of Atmospheric Sciences, Pusan National University, Busan 46241, South Korea

^c Institute for Future Earth, Pusan National University, Busan 46241, South Korea

ARTICLE INFO

Keywords:

Urban heat island
Background temperature
Background humidity
Thermodynamic process
Heat wave
Climate change

ABSTRACT

This study investigates changes in urban heat island (UHI) intensity with background temperature and humidity and their associations with physical processes. For this, we conducted idealized ensemble simulations with different initial potential temperature and water vapor mixing ratio profiles using the Weather Research and Forecasting (WRF) model. The daytime and nighttime UHI intensities increase with increasing background temperature at rates of $0.03\text{ }^{\circ}\text{C }^{\circ}\text{C}^{-1}$ and $0.20\text{ }^{\circ}\text{C }^{\circ}\text{C}^{-1}$, respectively. The daytime and nighttime UHI intensities decrease with increasing background humidity at rates of $-0.01\text{ }^{\circ}\text{C }(\text{g kg}^{-1})^{-1}$ and $-0.28\text{ }^{\circ}\text{C }(\text{g kg}^{-1})^{-1}$, respectively. The increase in background temperature increases the radiative cooling of rural air, enhancing the evening rural 2-m temperature decline. This also decreases the radiative heating of urban air and increases urban advective cooling, but decreases urban turbulent mixing. Consequently, the evening urban 2-m temperature decline is less enhanced, increasing the nighttime UHI intensity. The increase in background humidity decreases the radiative cooling of rural air, weakening the evening rural 2-m temperature decline. This also increases the radiative heating of urban air and decreases urban advective cooling, but increases urban turbulent mixing. Consequently, the evening urban 2-m temperature decline is less weakened, decreasing the nighttime UHI intensity.

1. Introduction

One of the biggest problems caused by climate change is the increase in heat stress (Sherwood and Huber, 2010). As both air temperature and absolute humidity have concurrently increased due to climate change, most regions across the world have experienced substantial increases in heat stress (Willett and Sherwood, 2012). Moreover, climate change is known to be responsible for increases in the frequency, intensity, and duration of heat waves (Perkins et al., 2012). In recent years, record-breaking heat waves occurred in many regions across the world, leading to numerous heat-related deaths (Aadhar and Mishra, 2023; White et al., 2023).

The increase in heat stress due to heat waves and climate change could be greater in urban areas than in rural areas (Fischer et al., 2012). This is because of the urban heat island (UHI) which refers to a phenomenon that the temperature in urban areas is higher than that in their surrounding rural areas (Qian et al., 2022). The UHI can synergistically interact with heat waves, possibly leading to

* Corresponding author.

E-mail address: jjbaik@snu.ac.kr (J.-J. Baik).

greater increases in heat stress due to heat waves in urban areas than in rural areas (Li and Bou-Zeid, 2013). The synergistic UHI-heat wave interaction occurs in many large cities around the world (Ramamurthy et al., 2017; Zhao et al., 2018; Jiang et al., 2019; Possega et al., 2022; Park et al., 2023). Ramamurthy et al. (2017) showed that the UHI intensity in New York City, U.S.A. is stronger by 2–3 °C during heat waves than during non-heat waves. Possega et al. (2022) showed that the UHI intensities in 28 European cities are on average stronger by 0.7 °C during heat waves than during non-heat waves.

Changes in UHI intensity with climate change have also been investigated in previous studies (Oleson et al., 2011; Lauwaet et al., 2016; Sachindra et al., 2016; Katzfey et al., 2020). Sachindra et al. (2016) showed that the UHI intensity in Melbourne, Australia overall increases under the Special Report on Emissions Scenarios (SRES) A2 scenario (a high emission scenario). Katzfey et al. (2020) showed that the nighttime UHI intensities in heavily urbanized areas increase under the Representative Concentration Pathways (RCP) 8.5 scenario (a high emission scenario). On the other hand, Oleson et al. (2011) showed that the UHI intensities in most urban areas decrease under the SRES A2 scenario. Similarly, Lauwaet et al. (2016) showed that the UHI intensity in Brussels, Belgium decreases under the RCP4.5 and RCP8.5 scenarios.

The abovementioned issues raise the following question: “How does the UHI intensity change with background temperature and humidity?” There are a few studies that examined changes in UHI intensity with background temperature (Scott et al., 2018; Gao et al., 2019; Sarangi et al., 2021). Scott et al. (2018) analyzed the UHI intensities in 54 cities in U.S.A. for 2000–2015 and showed that the UHI intensities in most cities decrease with increasing background temperature. Gao et al. (2019) showed that both daytime and nighttime UHI intensities in Beijing, China during the summer increase with increasing background temperature at rates of 0.0207 (0.0569) °C °C⁻¹ and 0.0715 (0.0995) °C °C⁻¹ in 2000 (2010), respectively. They suggested that the increase in the urban-rural difference in latent heat flux with increasing background temperature is a main reason for the positive sensitivities of the UHI intensities to background temperature. Some studies investigated changes in UHI intensity with background humidity and showed that the UHI intensity is negatively correlated with relative humidity (Hoffmann et al., 2012; Schatz and Kucharik, 2014; Arnds et al., 2017; Liu et al., 2020). Hoffmann et al. (2012) suggested that an increase in relative humidity tends to increase condensational heating during the nighttime particularly in rural areas, thereby decreasing the UHI intensity. Schatz and Kucharik (2014) suggested that an increase in relative humidity leads to an increase in the thermal admittance of air which can decrease the urban-rural difference in the heating/cooling rate of air.

Despite several studies of changes in UHI intensity with background temperature and humidity, their associations with physical processes are yet to be well understood. Furthermore, even though near-surface thermodynamic processes that include radiative heating/cooling of air, turbulent mixing, and advection in urban and rural areas significantly vary with background temperature and humidity (Sánchez et al., 2007; Holmes et al., 2016; Kim et al., 2024) and this may crucially affect the UHI intensity (Pigeon et al., 2007; Ren and Stroud, 2020), this aspect has not been explored.

This study aims to better understand changes in UHI intensity with background temperature and humidity through examining near-surface thermodynamic processes as well as surface energy fluxes. For this, idealized ensemble simulations are performed. Based on the analysis results, some implications for changes in UHI intensity under heat waves and climate change are provided.

2. Numerical model, simulation set-up, and analysis method

In this study, the Weather Research and Forecasting (WRF) model version 4.1.3 (Skamarock et al., 2019) is employed to perform idealized ensemble simulations. We considered a two-dimensional idealized mode in which full physical processes are taken into account. The horizontal extent and vertical extent of the domain are 200 km and 7 km, respectively. The number of grid points is 400 in the horizontal direction and 66 in the vertical direction. There are 34 vertical levels within the lowermost 1 km layer. The urban area whose half-width is 10 km is situated in the central area of the computational domain, and the rest of the domain is the rural area

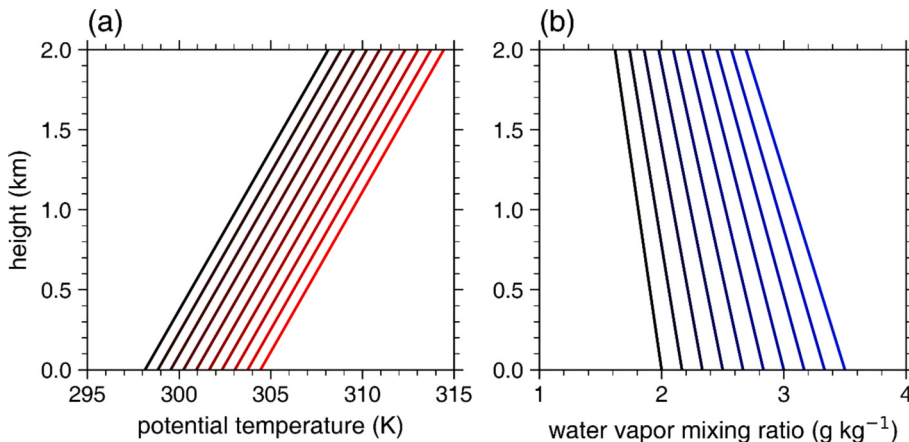


Fig. 1. (a) 10 different initial potential temperature profiles used in the experiments. (b) 10 different initial water vapor mixing ratio profiles used in the experiments.

(cropland/woodland mosaic). The midlatitude (30°N) is considered. In the lateral directions, the periodic boundary conditions are applied. The Coriolis effect is not included. For physics parameterizations, the Dudhia shortwave radiation scheme (Dudhia, 1989), the Rapid Radiative Transfer Model (RRTM) longwave radiation scheme (Mlawer et al., 1997), the WRF single-moment 6-class micro-physics scheme (Hong and Lim, 2006), the Yonsei University planetary boundary layer (PBL) scheme (Hong et al., 2006), the revised MM5 surface-layer similarity scheme (Jiménez et al., 2012), the unified Noah land surface model (LSM) (Chen and Dudhia, 2001), and the Seoul National University Urban Canopy Model (SNUUCM) (Ryu et al., 2011) are adopted. The SNUUCM represents the built-up surface as a roof, two facing walls, and a road and considers a single representative property for each facet (a single-layer approach). The SNUUCM divides the two facing walls into the sunlit wall and the shaded wall and separately calculates the surface temperature of each wall. To simulate physical processes occurring at the natural surface in urban areas, the unified Noah LSM is coupled with the SNUUCM in a tile approach. The SNUUCM was evaluated in intercomparison projects of urban land surface models (Grimmond et al., 2010; Grimmond et al., 2011; Lipson et al., 2024) and showed good performances in simulating urban surface energy fluxes. The values of urban morphological and thermal parameters used in this study are the same as those in Ryu and Baik (2012), except for a built-up area fraction of 0.9, a mean building height of 10 m, a road width of 10 m, a roof width of 10 m, and roof, wall, and road albedos of 0.18. In addition, a profile of diurnally varying anthropogenic heat flux whose daily mean, minimum, and maximum values are, respectively, 50 W m^{-2} , 6 W m^{-2} , and 90 W m^{-2} (Chen et al., 2011) is applied to the urban area.

Total 100 experiments are conducted using 10 different initial potential temperature (θ) profiles and 10 different initial water vapor mixing ratio (q) profiles. Fig. 1a shows the 10 different initial θ profiles. The initial surface potential temperature (θ_{sfc}) varies from 298.15 K ($25.0\text{ }^{\circ}\text{C}$) to 304.45 K ($31.3\text{ }^{\circ}\text{C}$) with a 0.7 K interval. For all initial θ profiles, the rate of change in θ with height is 5 K km^{-1} . The 10 different w profiles are presented in Fig. 1b. For all initial q profiles, q linearly decreases with increasing height and is 0.83 g kg^{-1} at the model top height. The initial surface water vapor mixing ratio (q_{sfc}) varies from 2.0 g kg^{-1} to 3.5 g kg^{-1} with a 0.167 g kg^{-1} interval. No initial background wind is considered, and no clouds appear in all experiments. The model integration period is from 0000 LST 21 June to 0500 LST 23 June, and the 24-h period from 0500 LST 22 June is analyzed. Each experiment consists of 10 ensemble simulations. For each ensemble member, perturbations of θ randomly sampled within the range between -0.1 K and 0.1 K are added to the lowest three levels of the initial θ field. The ensemble-mean result for each experiment is used for analysis. Note that in this study, 1000 simulations are conducted to examine changes in UHI intensity with background temperature and humidity.

In this study, the UHI intensity is calculated by subtracting the 2-m temperature averaged over the rural area from the 2-m temperature averaged over the urban area. Previous studies pointed out that the 2-m temperature diagnosed in the WRF model does not truly represent the temperature at 2-m height in urban areas but this is usable as a representative near-surface air temperature (Li and Bou-Zeid, 2014; Li et al., 2014). Following Ryu and Baik (2012), the daytime (nighttime) average is calculated using data over 1200–1700 LST (0000–0500 LST). The background temperature (humidity) is defined as the 2-m temperature (2-m water vapor mixing ratio) averaged over all grids. The sensitivity of daytime/nighttime mean UHI intensity to background temperature is calculated as follows. First, for an initial q_{sfc} (e.g., 2.0 g kg^{-1}), the linear regression slope of daytime/nighttime mean UHI intensity against the daytime/nighttime mean background temperature is calculated using the data from 10 experiments with different initial θ_{sfc} . The same process is carried out for different initial q_{sfc} . Then, the average value of the calculated linear regression slopes is considered as the sensitivity. The sensitivity of daytime/nighttime mean UHI intensity to background humidity is calculated in a similar way.

To elucidate how changes in background temperature and humidity affect the UHI intensity, changes in surface energy fluxes and those in near-surface thermodynamic processes are examined in detail. For the latter, the thermodynamic energy equation in the

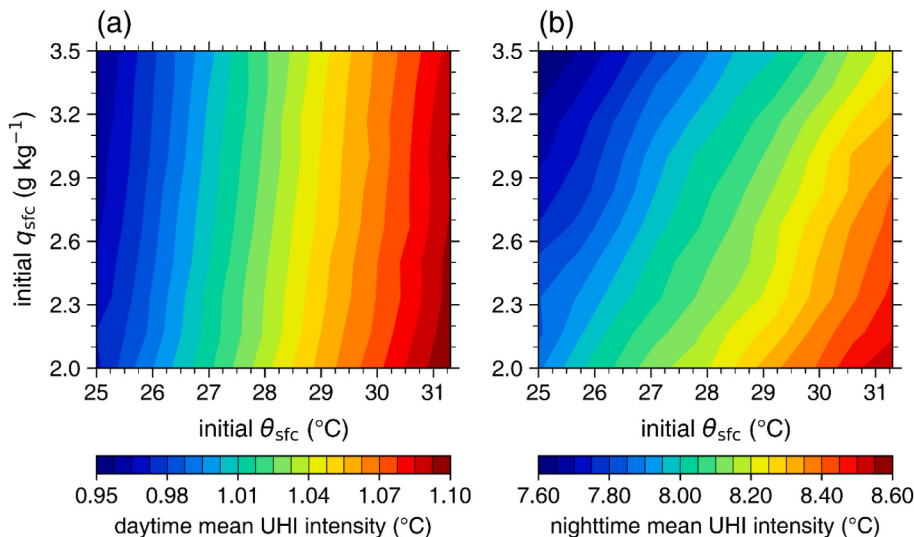


Fig. 2. (a) Daytime mean urban heat island intensity as a function of initial surface potential temperature and initial surface water vapor mixing ratio. (b) Same as (a) except for nighttime mean urban heat island intensity.

lowest model layer, whose mid-level is 13 m, is analyzed. The thermodynamic energy equation can be written as follows:

$$\frac{\partial \theta}{\partial t} = \left(\frac{\partial \theta}{\partial t} \right)_{RAD} + \left(\frac{\partial \theta}{\partial t} \right)_{PBL} + \left(\frac{\partial \theta}{\partial t} \right)_{MP} + \left(\frac{\partial \theta}{\partial t} \right)_{ADV} \quad (1)$$

where $\partial \theta / \partial t$ is the total θ tendency and $(\partial \theta / \partial t)_{RAD}$, $(\partial \theta / \partial t)_{PBL}$, $(\partial \theta / \partial t)_{MP}$, and $(\partial \theta / \partial t)_{ADV}$ are the θ tendencies due to the radiative processes, PBL processes, microphysical processes, and advection, respectively. $(\partial \theta / \partial t)_{MP}$ is neglected in the analysis since no clouds appear in the model atmosphere for all simulations. $(\partial \theta / \partial t)_{PBL}$ can be decomposed into the θ tendency due to the vertical turbulent mixing ($(\partial \theta / \partial t)_{MIX}$) and the θ tendency due to the surface sensible heat flux ($(\partial \theta / \partial t)_H$). Although Eq. (1) does not directly represent the 2-m temperature tendency, its analysis can help to understand near-surface thermodynamic processes. Previous studies pointed out that the influences of urban surface on the overlying atmosphere are more appropriately represented by the prognostic variables in the lowest model layer than by the diagnostic variables (e.g., 2-m temperature, 10-m wind velocity) in the WRF-single layer urban canopy model modeling system (Loridan et al., 2013; Sun et al., 2016).

3. Results and discussion

3.1. Changes in UHI intensity with background temperature and humidity

Fig. 2 shows the daytime mean and nighttime mean UHI intensities as a function of initial θ_{sfc} and q_{sfc} . The standard deviations of the UHI intensities in ensemble members of each experiment do not exceed 0.01 °C, indicating that the ensemble spread in each experiment does not affect the main results. As initial θ_{sfc} varies from 25.0 °C to 31.3 °C and initial q_{sfc} varies from 2.0 g kg⁻¹ to 3.5 g kg⁻¹, the daytime mean UHI intensity varies from 0.96 °C to 1.10 °C and the nighttime mean UHI intensity varies from 7.61 °C to 8.54 °C. Both daytime mean and nighttime mean UHI intensities increase with increasing initial θ_{sfc} and decrease with increasing initial q_{sfc} . The calculated sensitivities of daytime mean and nighttime mean UHI intensities to background temperature are 0.03 °C °C⁻¹ and 0.20 °C °C⁻¹, respectively. The calculated sensitivities of daytime mean and nighttime mean UHI intensities to background humidity are $-0.01^{\circ}\text{C} (\text{g kg}^{-1})^{-1}$ and $-0.28^{\circ}\text{C} (\text{g kg}^{-1})^{-1}$, respectively. These show that the nighttime mean UHI intensity much more prominently changes with background temperature and humidity than the daytime mean UHI intensity. This study finds the positive sensitivities of daytime and nighttime UHI intensities to background temperature that agree with Gao et al. (2019) and Sarangi et al. (2021). This suggests that the warming of the atmosphere acts to increase the UHI intensity. Furthermore, this study also finds the negative sensitivities of daytime and nighttime UHI intensities to background humidity in agreement with previous studies (e.g., Hu et al., 2019; Peng et al., 2019). This suggests that the moistening of the atmosphere acts to decrease the UHI intensity. Note that the results obtained from the simulations with the Shin-Hong scale-aware PBL scheme (Shin and Hong, 2015) are overall similar to the above results (Fig. A1 in Appendix A). In addition, the increases in the daytime mean and nighttime mean UHI intensities with increasing background temperature and the decreases in the daytime mean and nighttime mean UHI intensities with increasing background humidity are also found in the simulations in the presence of initial background wind (Fig. B1 in Appendix B). It is noted that the daytime (nighttime) mean urban 10-m wind speed in the CTRL experiment (see the next paragraph) is 3.5 m s⁻¹ (0.3 m s⁻¹) in the simulations with no initial background wind and 4.1 m s⁻¹ (0.4 m s⁻¹) in the simulations in which the initial background wind speed is 5 m s⁻¹.

In the next two subsections, changes in UHI intensity with background temperature and changes in UHI intensity with background humidity are separately investigated in detail. To examine changes in UHI intensity with background temperature, the experiment with the profiles in which θ_{sfc} is 25.0 °C and q_{sfc} is 2.0 g kg⁻¹ and the experiment with the profiles in which θ_{sfc} is 31.3 °C and q_{sfc} is 2.0

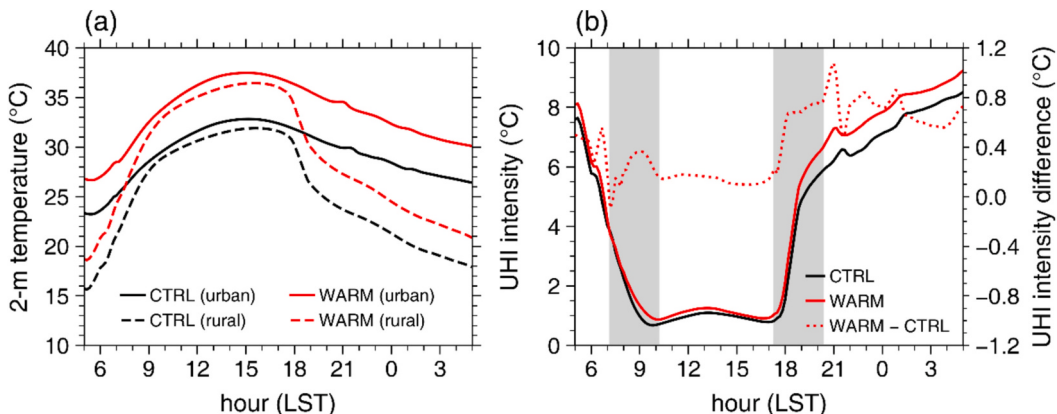


Fig. 3. (a) Diurnal variations of urban (solid) and rural (dashed) 2-m temperatures in the CTRL (black) and WARM (red) experiments. (b) Diurnal variations of urban heat island intensities in the CTRL (black) and WARM (red) experiments. The red dotted line indicates the difference between the two experiments (WARM minus CTRL). The shaded areas indicate 0710–1010 LST and 1720–2020 LST. (For interpretation of the references to colour in this figure legend, the reader is referred to the web version of this article.)

g kg^{-1} are compared. The former experiment is called the “CTRL” experiment, and the latter one is called the “WARM” experiment. To examine changes in UHI intensity with background humidity, the CTRL experiment and the experiment with the profiles in which θ_{sfc} is 25.0°C and q_{sfc} is 3.5 g kg^{-1} , called the MOIST experiment, are compared.

3.2. Changes in UHI intensity with background temperature and their associations with physical processes

Fig. 3a shows the urban and rural 2-m temperatures in the CTRL and WARM experiments. In both experiments, the urban and rural 2-m temperatures exhibit clear diurnal variations. In the CTRL experiment, the diurnal temperature range (DTR) is 9.6°C in the urban area and 16.3°C in the rural area. The smaller DTR in urban areas than in their surrounding rural areas has been observed in many cities (Türkcs and Sümer, 2004; Wang et al., 2012). As the background temperature increases, both urban and rural 2-m temperatures increase throughout the day (Fig. 3a). Compared to the CTRL experiment, the mean urban (rural) 2-m temperature in the WARM experiment is higher by 4.65°C (4.52°C) during the daytime and by 3.79°C (3.14°C) during the nighttime. This shows that the urban area experiences more warming than the rural area as the background temperature increases.

Fig. 3b shows the UHI intensities in the CTRL and WARM experiments. In both experiments, the UHI intensity is much stronger during the nighttime than during the daytime, consistent with previous studies (Oke, 1982; Basara et al., 2008). In comparison with the CTRL experiment, the mean UHI intensity in the WARM experiment is stronger by 0.13°C during the daytime and by 0.66°C during the nighttime. The difference in UHI intensity between the CTRL and WARM experiments (WARM minus CTRL) clearly increases in the

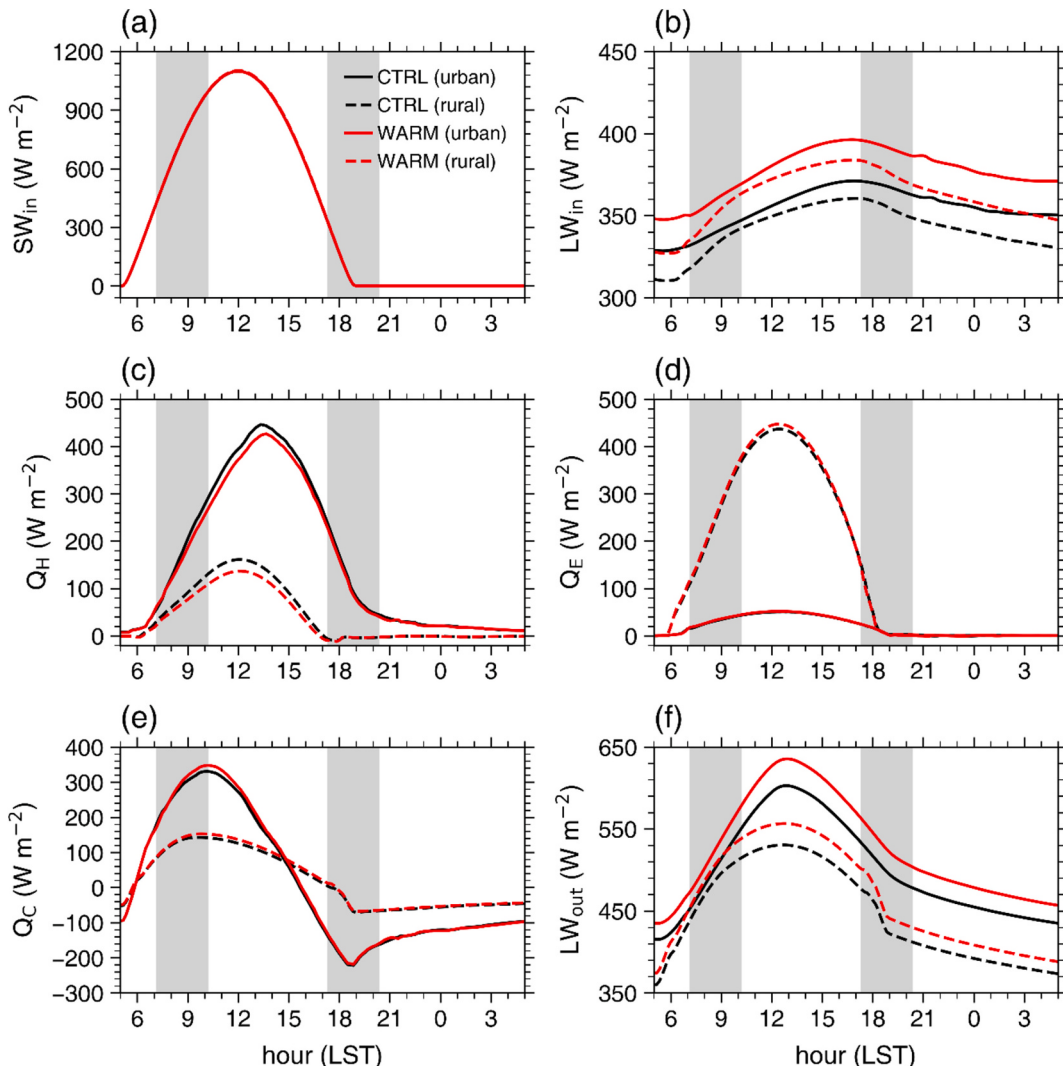


Fig. 4. Diurnal variations of urban (solid) and rural (dashed) (a) incoming shortwave radiation (SW_{in}), (b) incoming longwave radiation (LW_{in}), (c) sensible heat flux (Q_H), (d) latent heat flux (Q_E), (e) storage heat flux (Q_C), and (f) outgoing longwave radiation (LW_{out}) in the CTRL (black) and WARM (red) experiments. The shaded areas indicate 0710–1010 LST and 1720–2020 LST. (For interpretation of the references to colour in this figure legend, the reader is referred to the web version of this article.)

morning and evening (Fig. 3b). During 0710–1010 LST, the difference in UHI intensity between the CTRL and WARM experiments increases from $-0.09\text{ }^{\circ}\text{C}$ to $0.16\text{ }^{\circ}\text{C}$. During 0710–1010 LST, the rise in urban 2-m temperature is larger by $1.22\text{ }^{\circ}\text{C}$ in the WARM experiment than in the CTRL experiment while the rise in rural 2-m temperature is larger only by $0.97\text{ }^{\circ}\text{C}$ in the WARM experiment than in the CTRL experiment (Fig. 3a). This shows that the increase in background temperature more enhances the rise in urban 2-m temperature than the rise in rural 2-m temperature in the morning, leading to the increase in daytime UHI intensity. During 1720–2020 LST, the difference in UHI intensity between the CTRL and WARM experiments increases from $0.22\text{ }^{\circ}\text{C}$ to $0.77\text{ }^{\circ}\text{C}$. During 1720–2020 LST, the decline in rural 2-m temperature is larger by $0.74\text{ }^{\circ}\text{C}$ in the WARM experiment than in the CTRL experiment while the decline in urban 2-m temperature is larger only by $0.19\text{ }^{\circ}\text{C}$ in the WARM experiment than in the CTRL experiment (Fig. 3a). This shows that the increase in background temperature more enhances the decline in rural 2-m temperature than the decline in urban 2-m temperature in the evening and thus results in the increase in nighttime UHI intensity.

The urban and rural surface energy fluxes in the CTRL and WARM experiments are compared in Fig. 4. In both experiments, the amounts of urban and rural incoming shortwave radiations are very similar and peak at 1200 LST (Fig. 4a). It is also found that the amounts of urban and rural incoming shortwave radiations hardly change with background temperature (Fig. 4a). The amount of urban incoming longwave radiation is larger than that of rural incoming longwave radiation in both experiments (Fig. 4b). This is mainly due to that the amount of incoming longwave radiation increases with increasing air temperature (Swinbank, 1963). For the same reason, the amounts of urban and rural incoming longwave radiations increase as the background temperature increases (Fig. 4b).

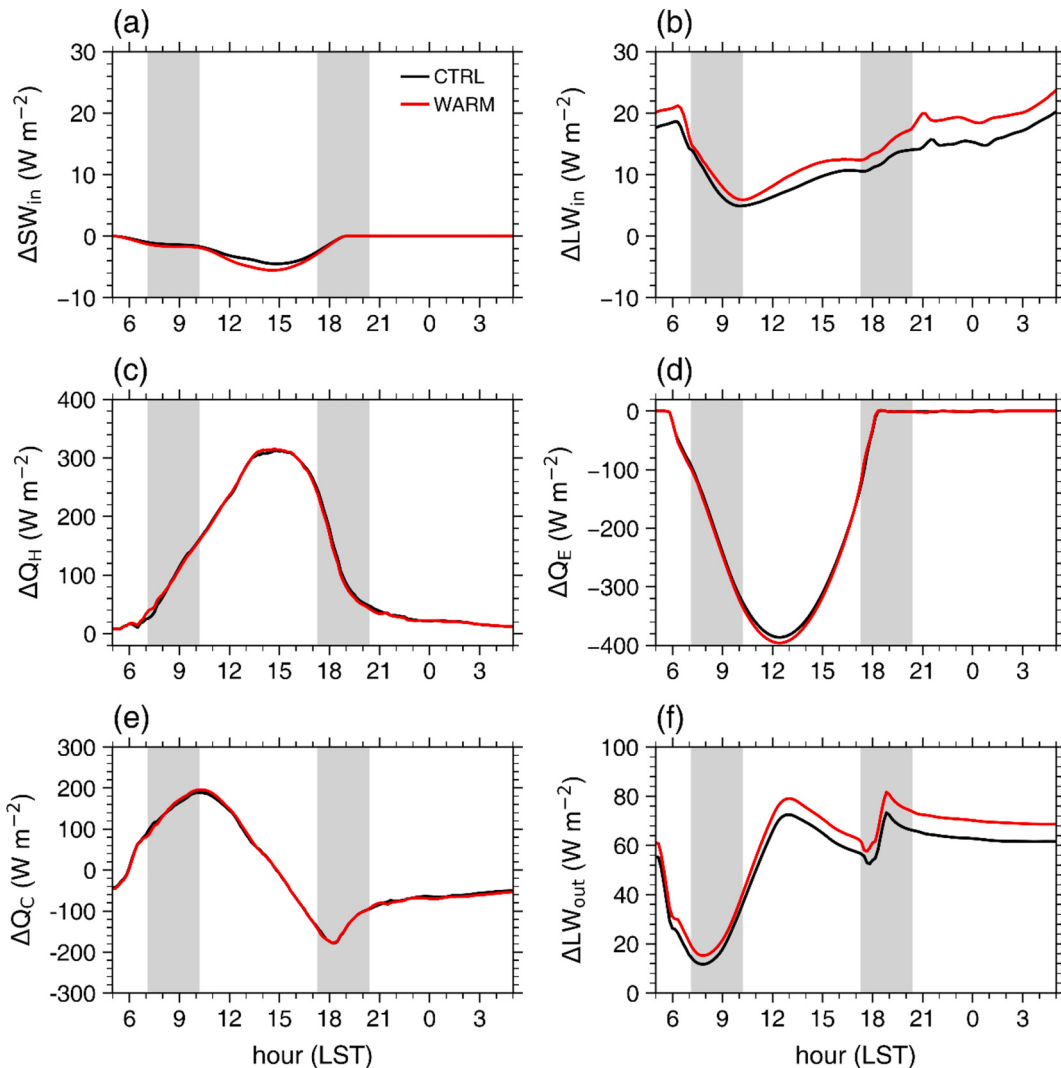


Fig. 5. Same as Fig. 4 except for the urban-rural differences in (a) incoming shortwave radiation (ΔSW_{in}), (b) incoming longwave radiation (ΔLW_{in}), (c) sensible heat flux (ΔQ_H), (d) latent heat flux (ΔQ_E), (e) storage heat flux (ΔQ_C), and (f) outgoing longwave radiation (ΔLW_{out}) in the CTRL (black) and WARM (red) experiments. (For interpretation of the references to colour in this figure legend, the reader is referred to the web version of this article.)

In both experiments, the sensible (latent) heat flux is larger (smaller) in the urban area than in the rural area (Fig. 4c and d). The dominant sensible heat flux over latent heat flux is a distinct characteristic of urban surface compared to vegetated rural surface (Cleugh and Oke, 1986; Li et al., 2015). Interestingly, the urban and rural sensible heat fluxes overall decrease as the background temperature increases (Fig. 4c). The daytime mean urban and rural sensible heat fluxes are smaller in the WARM experiment than in the CTRL experiment by 17.6 W m^{-2} and 18.9 W m^{-2} , respectively. These changes are in contrast with changes in sensible heat flux which typically appear during heat waves (Zaitchik et al., 2006; Ao et al., 2019). This is possibly due to that only increase in initial air temperature is considered in the WARM experiment. As a result, the differences between the surface temperature and 2-m temperature in both urban and rural areas are overall smaller in the WARM experiment than in the CTRL experiment (not shown). On the other hand, the urban and rural latent heat fluxes overall slightly increase as the background temperature increases (Fig. 4d). The daytime mean urban and rural latent heat fluxes are larger in the WARM experiment than in the CTRL experiment by 0.6 W m^{-2} and 7.1 W m^{-2} , respectively.

In both experiments, the magnitude of urban storage heat flux is generally much larger than that of rural storage heat flux throughout the day (Fig. 4e), consistent with previous studies (Wang et al., 2020; Zhou et al., 2024). As the background temperature increases, the storage heat flux increases during the daytime and slightly changes during the nighttime in both urban and rural areas (Fig. 4e). The daytime mean urban and rural storage heat fluxes are larger in the WARM experiment than in the CTRL experiment by 10.6 W m^{-2} and 9.4 W m^{-2} , respectively. The magnitude of nighttime mean urban (rural) storage heat flux is slightly larger (smaller) in the WARM experiment than in the CTRL experiment by 1.5 W m^{-2} (2.2 W m^{-2}). Meanwhile, the amount of urban outgoing longwave radiation is consistently larger than that of rural outgoing longwave radiation in both experiments (Fig. 4f). This is mainly due to the higher urban surface temperature than the rural surface temperature. As the background temperature increases, the amounts of urban and rural outgoing longwave radiations increase throughout the day (Fig. 4f).

The urban-rural differences in surface energy fluxes are main factors contributing to the UHI (Oke et al., 2017). Fig. 5 is the same as Fig. 4 except for the urban-rural differences in the energy fluxes in the CTRL and WARM experiments. It is notable that in the morning and evening when the difference in UHI intensity between the CTRL and WARM experiments clearly increases (Fig. 3b), there are no distinct increases in the urban-rural differences in the energy fluxes with increasing background temperature compared to other times of the day (Fig. 5). This implies that the increases in daytime and nighttime UHI intensities with increasing background temperature are associated with changes in other physical processes rather than those in surface energy fluxes.

Fig. 6 shows the diurnal variations of the urban-rural difference in θ ($\Delta\theta$) and urban and rural $\partial\theta/\partial t$ in the lowest model layer in the CTRL and WARM experiments. In both experiments, $\Delta\theta$ in the lowest model layer is much larger during the nighttime than during the daytime (Fig. 6a), consistent with the UHI intensity (Fig. 3b). Moreover, the difference in $\Delta\theta$ between the two experiments (WARM minus CTRL) in the lowest model layer clearly increases in the morning and evening (Fig. 6a), consistent with the difference in UHI intensity between the two experiments (Fig. 3b). The difference in $\Delta\theta$ between the two experiments in the lowest model layer increases from -0.16°C to 0.18°C during 0710–1010 LST and increases from 0.12°C to 0.63°C during 1720–2020 LST. The rise in urban θ in the morning in the lowest model layer and the decline in rural θ in the evening in the lowest model layer are prominently enhanced with increasing background temperature (Fig. 6b), consistent with Fig. 3a. The mean differences in urban and rural $\partial\theta/\partial t$ between the two experiments in the lowest model layer are 0.36 K h^{-1} and 0.31 K h^{-1} during 0710–1010 LST and -0.03 K h^{-1} and -0.22 K h^{-1} during 1720–2020 LST, respectively. Thus, Fig. 6 indicates that analyzing thermodynamic processes in the lowest model layer can provide insights into changes in UHI intensity with background temperature.

The thermodynamic processes in the lowest model layer are examined in detail. Fig. 7 shows the diurnal variations of urban and rural $(\partial\theta/\partial t)_{\text{RAD}}$, $(\partial\theta/\partial t)_{\text{PBL}}$, and $(\partial\theta/\partial t)_{\text{ADV}}$ in the lowest model layer in the CTRL and WARM experiments. In both experiments, the

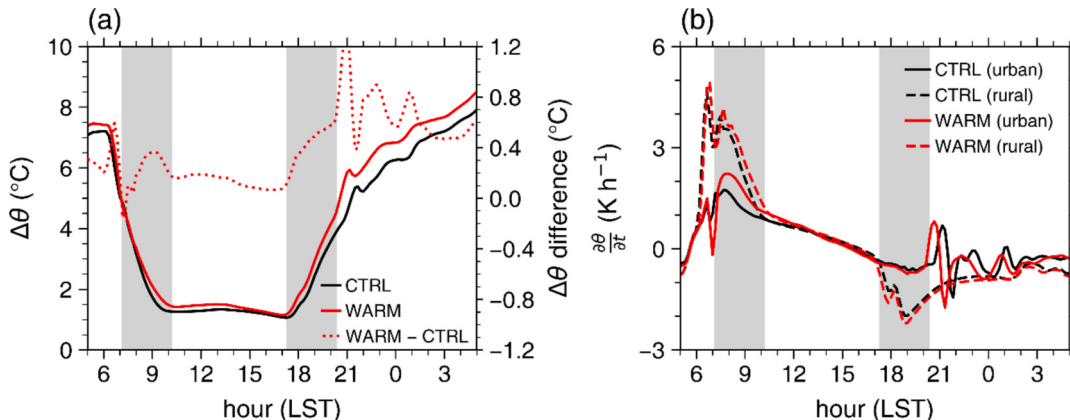


Fig. 6. (a) Diurnal variations of the urban-rural differences in potential temperature in the lowest model layer in the CTRL (black) and WARM (red) experiments. The red dotted line indicates the difference between the two experiments (WARM minus CTRL). (b) Diurnal variations of urban (solid) and rural (dashed) potential temperature tendencies in the lowest model layer in the CTRL (black) and WARM (red) experiments. The shaded areas indicate 0710–1010 LST and 1720–2020 LST. (For interpretation of the references to colour in this figure legend, the reader is referred to the web version of this article.)

positive $(\partial\theta/\partial t)_{RAD}$ appears later in the urban area than in the rural area (Fig. 7a), indicating that the radiative heating of urban air occurs later than that of rural air. During the daytime, the urban $(\partial\theta/\partial t)_{RAD}$ is much stronger than the rural $(\partial\theta/\partial t)_{RAD}$. This is associated with the larger amount of urban outgoing longwave radiation than that of rural outgoing longwave radiation (Fig. 4f). The negative $(\partial\theta/\partial t)_{RAD}$ also appears later in the urban area than in the rural area (Fig. 7a), indicating that the radiative cooling of urban air occurs later than that of rural air. The urban and rural $(\partial\theta/\partial t)_{PBL}$ are positive during 0610–0900 LST (Fig. 7b). This results from the stronger heating of air by the sensible heat flux (Fig. 4c) than the cooling of air by the turbulent mixing. As the PBL well develops during the daytime, the urban and rural $(\partial\theta/\partial t)_{PBL}$ are negative. The negative $(\partial\theta/\partial t)_{PBL}$ during the daytime is much stronger in the urban area than in the rural area despite the larger urban sensible heat flux (Fig. 4c). This indicates that the urban turbulent mixing is much stronger than the rural turbulent mixing during the daytime, leading to the stronger cooling tendency due to the PBL processes in the urban area than in the rural area. After 1800 LST, the urban $(\partial\theta/\partial t)_{PBL}$ is positive while the rural $(\partial\theta/\partial t)_{PBL}$ is very small. This is related to the urban sensible heat flux still appearing after 1800 LST (Fig. 4c). The rural $(\partial\theta/\partial t)_{ADV}$ is very minor except during the daytime (Fig. 7c) when the urban breeze circulation well develops. The urban $(\partial\theta/\partial t)_{ADV}$ is negative throughout the day.

During 0710–1010 LST, the mean differences in urban $(\partial\theta/\partial t)_{RAD}$, $(\partial\theta/\partial t)_{PBL}$, and $(\partial\theta/\partial t)_{ADV}$ between the CTRL and WARM experiments (WARM minus CTRL) are 0.01 K h^{-1} , 0.61 K h^{-1} , and -0.27 K h^{-1} , respectively (Fig. 7 and Fig. C1 in Appendix C). The positive mean difference in urban $(\partial\theta/\partial t)_{PBL}$ is prominent despite the smaller urban sensible heat flux in the WARM experiment than in the CTRL experiment during 0710–1010 LST (Fig. 4c). This is attributed to that the urban turbulent mixing during 0710–1010 LST is weaker in the WARM experiment than in the CTRL experiment (Fig. C2 in Appendix C). Thus, these results suggest that the prominently enhanced rise in urban 2-m temperature during 0710–1010 LST with increasing background temperature (Fig. 3a), which leads to the increase in daytime UHI intensity, is primarily attributed to the decrease in urban turbulent mixing with increasing background temperature. Meanwhile, the mean differences in rural $(\partial\theta/\partial t)_{RAD}$, $(\partial\theta/\partial t)_{PBL}$, and $(\partial\theta/\partial t)_{ADV}$ between the CTRL and WARM experiments during 0710–1010 LST are 0.01 K h^{-1} , 0.24 K h^{-1} , and 0.06 K h^{-1} , respectively (Fig. 7 and Fig. C1 in Appendix C). The positive mean difference in rural $(\partial\theta/\partial t)_{PBL}$ is much less prominent than that in urban $(\partial\theta/\partial t)_{PBL}$, which is responsible for the less enhanced rise in rural 2-m temperature during 0710–1010 LST with increasing background temperature (Fig. 3a).

During 1720–2020 LST, the mean difference in rural $(\partial\theta/\partial t)_{RAD}$ between the CTRL and WARM experiments is -0.22 K h^{-1} (Fig. 7a and Fig. C1a in Appendix C). This means that the radiative cooling of rural air during 1720–2020 LST is stronger in the WARM experiment than in the CTRL experiment. The increase in background temperature increases the emissions of longwave radiation from the atmosphere. The mean differences in rural $(\partial\theta/\partial t)_{PBL}$ and $(\partial\theta/\partial t)_{ADV}$ between the CTRL and WARM experiments are, respectively, -0.02 K h^{-1} and 0.02 K h^{-1} (Fig. 7b and c and Fig. C1b and c in Appendix C) and are much smaller than that in rural $(\partial\theta/\partial t)_{RAD}$. Thus, these results suggest that the prominently enhanced decline in rural 2-m temperature during 1720–2020 LST with increasing background temperature (Fig. 3a), which leads to the increase in nighttime UHI intensity, is primarily attributed to the increase in the

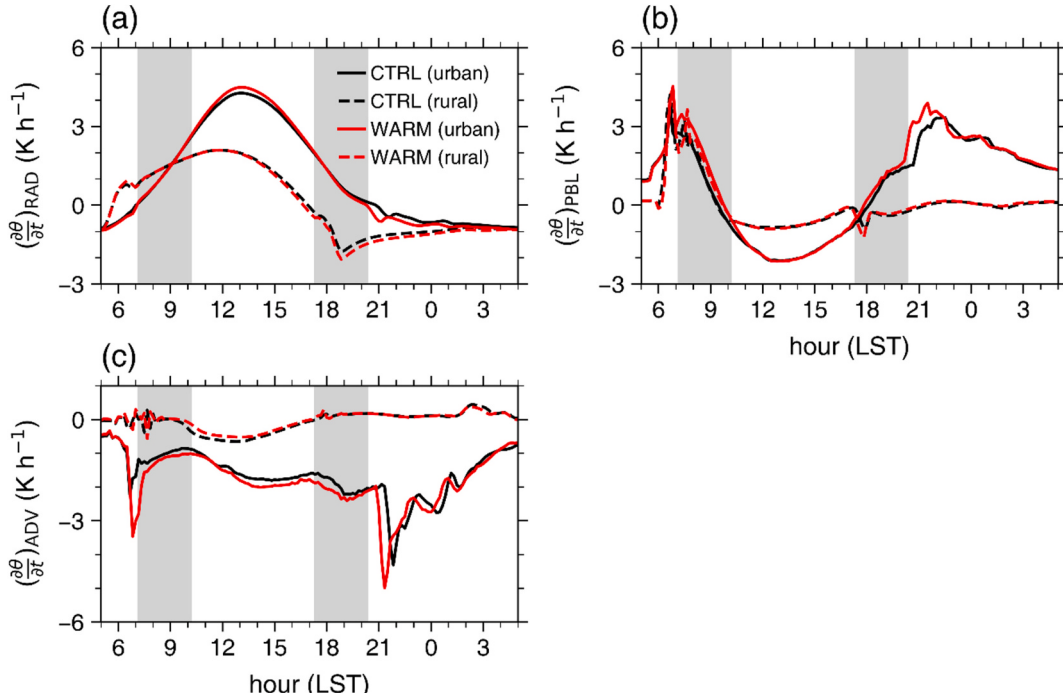


Fig. 7. Diurnal variations of urban (solid) and rural (dashed) potential temperature tendencies in the lowest model layer due to (a) radiative processes, (b) planetary boundary layer processes, and (c) advection in the CTRL (black) and WARM (red) experiments. The shaded areas indicate 0710–1010 LST and 1720–2020 LST. (For interpretation of the references to colour in this figure legend, the reader is referred to the web version of this article.)

radiative cooling of rural air with increasing background temperature. Meanwhile, the mean differences in urban $(\partial\theta/\partial t)_{RAD}$, $(\partial\theta/\partial t)_{PBL}$, and $(\partial\theta/\partial t)_{ADV}$ between the CTRL and WARM experiments during 1720–2020 LST are -0.05 K h^{-1} , 0.24 K h^{-1} , and -0.21 K h^{-1} , respectively (Fig. 7 and Fig. C1 in Appendix C). The radiative heating of urban air is weaker and the urban advective cooling is stronger in the WARM experiment than in the CTRL experiment. The positive mean difference in urban $(\partial\theta/\partial t)_{PBL}$ is also attributed to the weaker urban turbulent mixing in the WARM experiment than in the CTRL experiment (Fig. C2 in Appendix C). The negative mean differences in urban $(\partial\theta/\partial t)_{RAD}$ and $(\partial\theta/\partial t)_{ADV}$ are offset by the positive mean difference in urban $(\partial\theta/\partial t)_{PBL}$, which is responsible for the less enhanced decline in urban 2-m temperature during 1720–2020 LST with increasing background temperature (Fig. 3a).

The above analysis results indicate that changes in near-surface thermodynamic processes are important for those in UHI intensity with background temperature. This suggests an implication for the examination of the UHI-heat wave interaction. In previous studies of the UHI-heat wave interaction, the causes of the synergistic UHI-heat wave interaction were typically explained by changes in urban and rural surface energy fluxes during heat waves (e.g., Zong et al., 2021; Cui et al., 2023; Ma et al., 2024). For example, several studies suggested that the synergistic UHI-heat wave interaction during the nighttime results from more prominent increases in heat storage or anthropogenic heat in urban areas than in rural areas during heat waves (e.g., Li et al., 2015; He et al., 2020; Zou et al., 2021). However, this could not support that the declines in urban and rural air temperatures during the nighttime are larger during heat waves than during non-heat waves in their studies. We suggest that analyzing how near-surface thermodynamic processes change under heat waves helps to better understand the UHI-heat wave interaction.

3.3. Changes in UHI intensity with background humidity and their associations with physical processes

Fig. 8a shows the urban and rural 2-m temperatures in the MOIST experiment as well as those in the CTRL experiment. As the background humidity increases, both urban and rural 2-m temperatures slightly increase throughout the day (Fig. 8a). This is associated with the enhanced greenhouse effect due to the increase in water vapor amount (Inamdar and Ramanathan, 1998; Philipona et al., 2005). In comparison with the CTRL experiment, the mean urban (rural) 2-m temperature in the MOIST experiment is higher by 0.32°C (0.33°C) during the daytime and by 0.67°C (0.95°C) during the nighttime. This shows that the rural area experiences more warming than the urban area with increasing background humidity.

The UHI intensity in the MOIST experiment is compared with that in the CTRL experiment in Fig. 8b. Compared to the CTRL experiment, the mean UHI intensity in the MOIST experiment is weaker by 0.01°C during the daytime and by 0.28°C during the nighttime. The difference in UHI intensity between the CTRL and MOIST experiments clearly changes in the evening as well as in the morning (Fig. 8b). The difference in UHI intensity between the CTRL and MOIST experiments (MOIST minus CTRL) changes from -0.06°C to -0.36°C during 1730–2030 LST and changes from -0.16°C to -0.00°C during 0700–1000 LST. During 1730–2030 LST, the decline in rural 2-m temperature is smaller by 0.37°C in the MOIST experiment than in the CTRL experiment and the decline in urban 2-m temperature is smaller by 0.07°C in the MOIST experiment than in the CTRL experiment (Fig. 8a). This shows that the increase in background humidity more weakens the decline in rural 2-m temperature than the decline in urban 2-m temperature in the evening and thus leads to the decrease in nighttime UHI intensity. During 0700–1000 LST, the rise in rural 2-m temperature is smaller by 0.42°C in the MOIST experiment than in the CTRL experiment and the rise in urban 2-m temperature is smaller by 0.26°C in the MOIST experiment than in the CTRL experiment (Fig. 8a). This shows that the increase in background humidity more weakens the rise in rural 2-m temperature than the rise in urban 2-m temperature in the morning. This diminishes the decrease in UHI intensity which occurred in the previous evening, leading to the very slight decrease in daytime UHI intensity with increasing background humidity.

The urban and rural surface energy fluxes in the MOIST experiment are compared with those in the CTRL experiment in Fig. 9. The amounts of urban and rural incoming shortwave radiations slightly decrease as the background humidity increases (Fig. 9a). This is

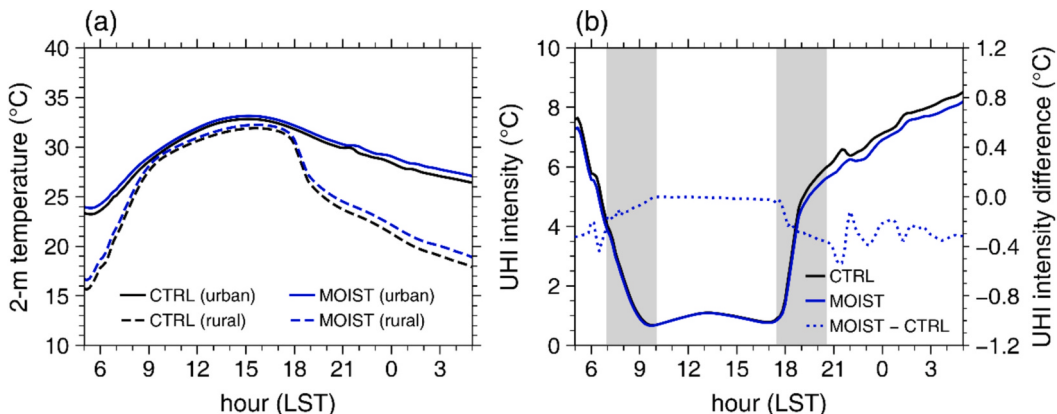


Fig. 8. (a) Diurnal variations of urban (solid) and rural (dashed) 2-m temperatures in the CTRL (black) and MOIST (blue) experiments. (b) Diurnal variations of urban heat island intensities in the CTRL (black) and MOIST (blue) experiments. The blue dotted line indicates the difference between the two experiments (MOIST minus CTRL). The shaded areas indicate 0700–1000 LST and 1730–2030 LST. (For interpretation of the references to colour in this figure legend, the reader is referred to the web version of this article.)

mainly due to the increase in absorption of shortwave radiation in the atmosphere which results from the increase in water vapor amount (Obregón et al., 2018; Salamalikis et al., 2021). As the background humidity increases, the amounts of urban and rural incoming longwave radiations increase throughout the day (Fig. 9b). Compared to the CTRL experiment, the mean amounts of urban and rural incoming longwave radiations in the MOIST experiment are larger by 11.8 W m^{-2} and 11.4 W m^{-2} during the daytime and by 11.7 W m^{-2} and 11.7 W m^{-2} during the nighttime, respectively. The urban and rural sensible (latent) heat fluxes during the daytime overall very slightly increase (decrease) as the background humidity increases (Fig. 9c and d). The magnitudes of urban and rural storage heat fluxes are overall very slightly smaller in the MOIST experiment than in the CTRL experiment throughout the day (Fig. 9e). The amounts of urban and rural outgoing longwave radiations also consistently increase as the background humidity increases (Fig. 9f). Compared to the CTRL experiment, the mean amounts of urban and rural outgoing longwave radiations in the MOIST experiment are larger by 3.3 W m^{-2} and 3.2 W m^{-2} during the daytime and 6.2 W m^{-2} and 7.1 W m^{-2} during the nighttime, respectively.

The increase in background humidity increases both incoming and outgoing longwave radiations, indicating that the greenhouse effect by water vapor is enhanced (Mitchell, 1989). Accordingly, the effect of changes in background humidity considered in this study implies the effect of changes in the greenhouse effect by water vapor. In previous studies that projected the decrease in UHI intensity with climate change due to the anthropogenic greenhouse effect, significant changes in the urban-rural differences in surface energy fluxes appear (e.g., Oleson et al., 2011; Chapman et al., 2019). On the other hand, in this study which only considers changes in background humidity under clear skies, there are no significant differences in the urban-rural differences in surface energy fluxes

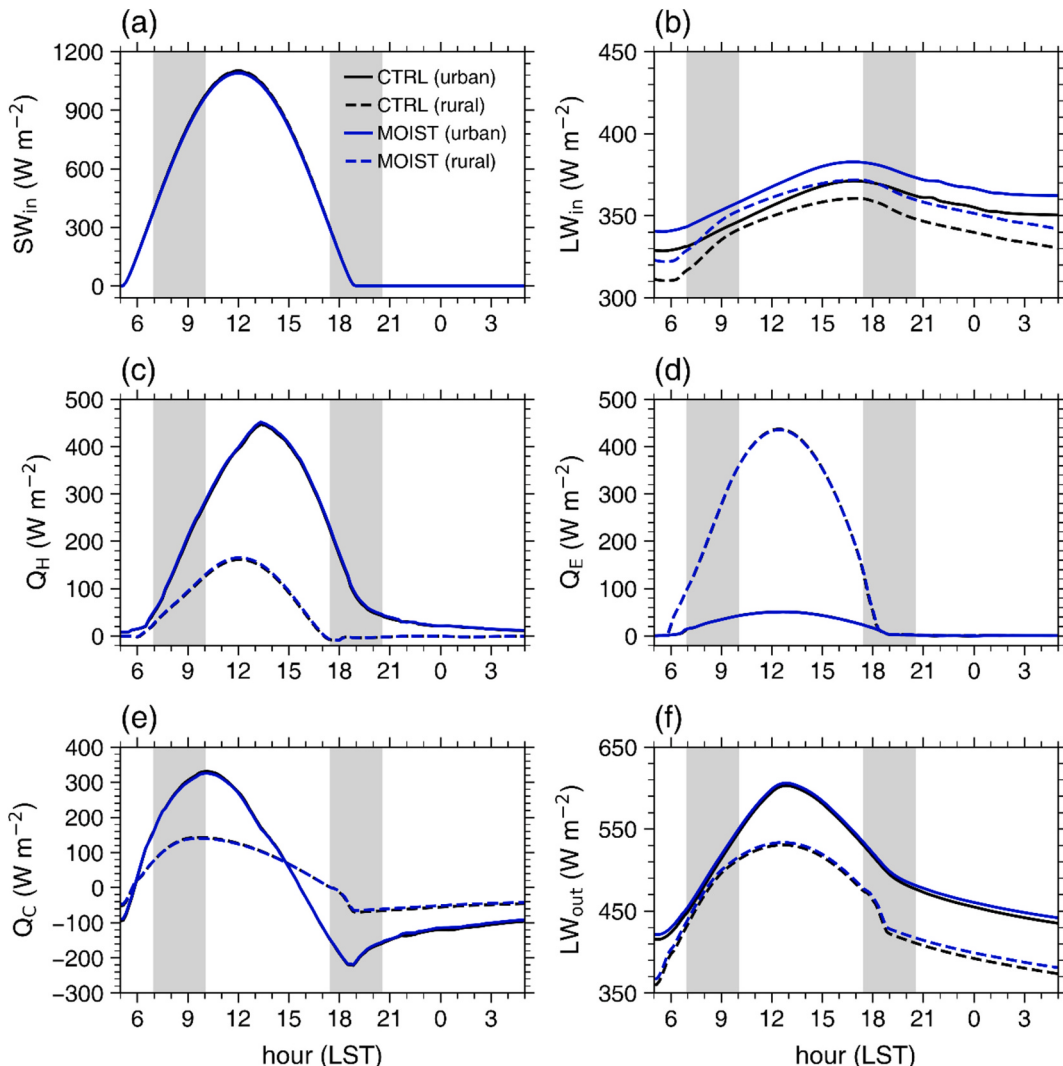


Fig. 9. Diurnal variations of urban (solid) and rural (dashed) (a) incoming shortwave radiation (SW_{in}), (b) incoming longwave radiation (LW_{in}), (c) sensible heat flux (Q_H), (d) latent heat flux (Q_E), (e) storage heat flux (Q_C), and (f) outgoing longwave radiation (LW_{out}) in the CTRL (black) and MOIST (blue) experiments. The shaded areas indicate 0700–1000 LST and 1730–2030 LST. (For interpretation of the references to colour in this figure legend, the reader is referred to the web version of this article.)

between the CTRL and MOIST experiments (Fig. 10). Notably, in the morning and evening when the difference in UHI intensity between the CTRL and MOIST experiments clearly changes (Fig. 8b), there are no associated changes in the urban-rural differences in surface energy fluxes with increasing background humidity. Nonetheless, it is interesting that the noticeable decrease in nighttime UHI intensity comparable to those in the previous studies appears as the background humidity increases. This implies that the decreases in daytime and nighttime UHI intensities with increasing background humidity are also associated with changes in other physical processes rather than those in surface energy fluxes.

Fig. 11 shows the diurnal variations of $\Delta\theta$ and urban and rural $\partial\theta/\partial t$ in the lowest model layer in the CTRL and MOIST experiments. The difference in $\Delta\theta$ between the two experiments (MOIST minus CTRL) in the lowest model layer exhibits very similar diurnal variation to that in UHI intensity (Figs. 8b and 11a). The difference in $\Delta\theta$ between the two experiments in the lowest model layer changes from -0.17°C to -0.01°C during 0700–1000 LST and changes from -0.04°C to -0.18°C during 1730–2030 LST. It is also found in the lowest model layer that the rise in rural θ in the morning and the decline in rural θ in the evening are prominently weakened with increasing background humidity (Fig. 11b), which is consistent with Fig. 8a. The mean differences in urban and rural $\partial\theta/\partial t$ between the two experiments in the lowest model layer are -0.07 K h^{-1} and -0.15 K h^{-1} during 0700–1000 LST and 0.02 K h^{-1} and 0.07 K h^{-1} during 1730–2030 LST, respectively. Therefore, Fig. 11 indicates that analyzing thermodynamic processes in the lowest model layer can help to understand changes in UHI intensity with background humidity.

Changes in thermodynamic processes in the lowest model layer with background humidity are examined in Fig. 12. In both urban and rural areas, the positive $(\partial\theta/\partial t)_{\text{RAD}}$ is generally stronger and the negative $(\partial\theta/\partial t)_{\text{RAD}}$ is generally weaker in the MOIST experiment

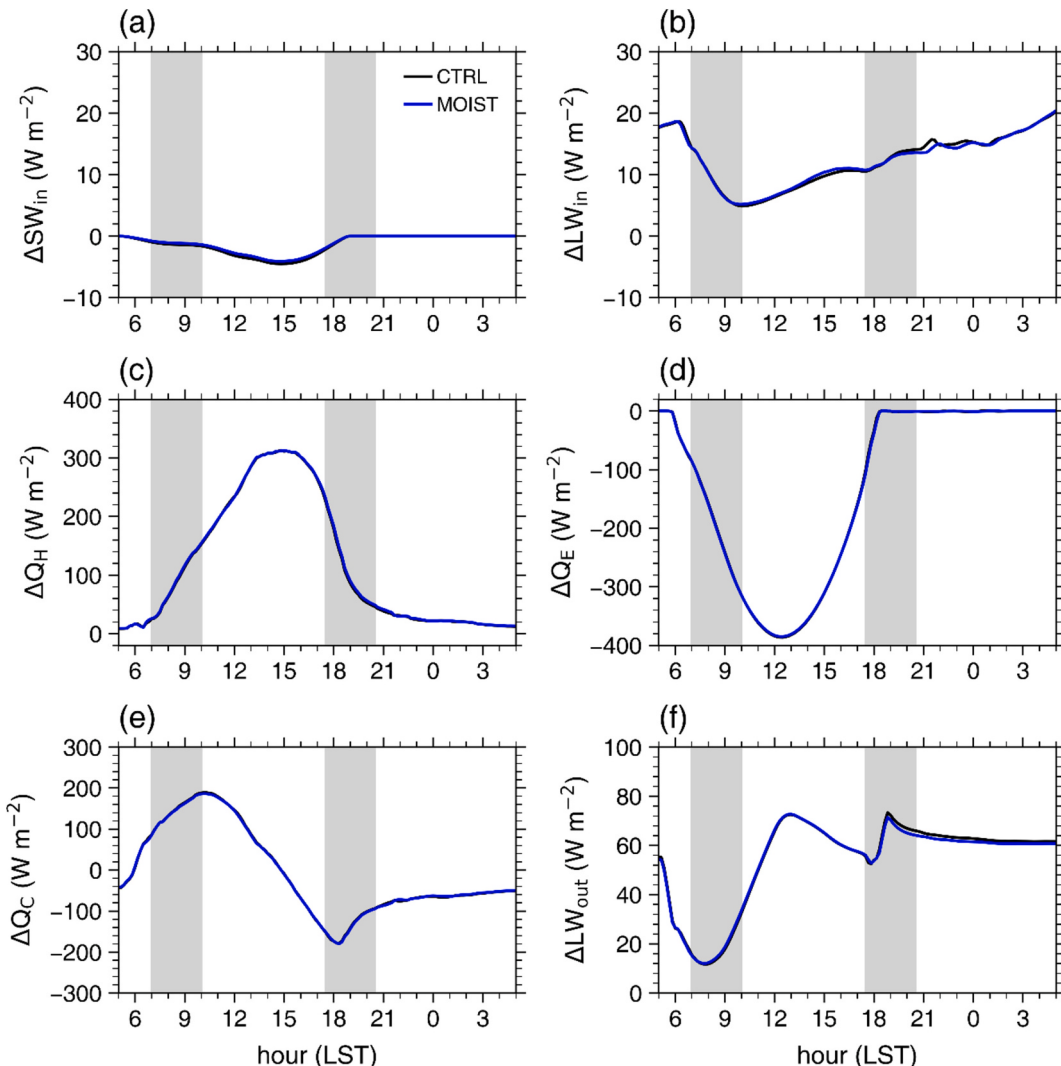


Fig. 10. Same as Fig. 9 except for the urban-rural differences in (a) incoming shortwave radiation ($\Delta\text{SW}_{\text{in}}$), (b) incoming longwave radiation ($\Delta\text{LW}_{\text{in}}$), (c) sensible heat flux (ΔQ_H), (d) latent heat flux (ΔQ_E), (e) storage heat flux (ΔQ_C), and (f) outgoing longwave radiation ($\Delta\text{LW}_{\text{out}}$) in the CTRL (black) and MOIST (blue) experiments. (For interpretation of the references to colour in this figure legend, the reader is referred to the web version of this article.)

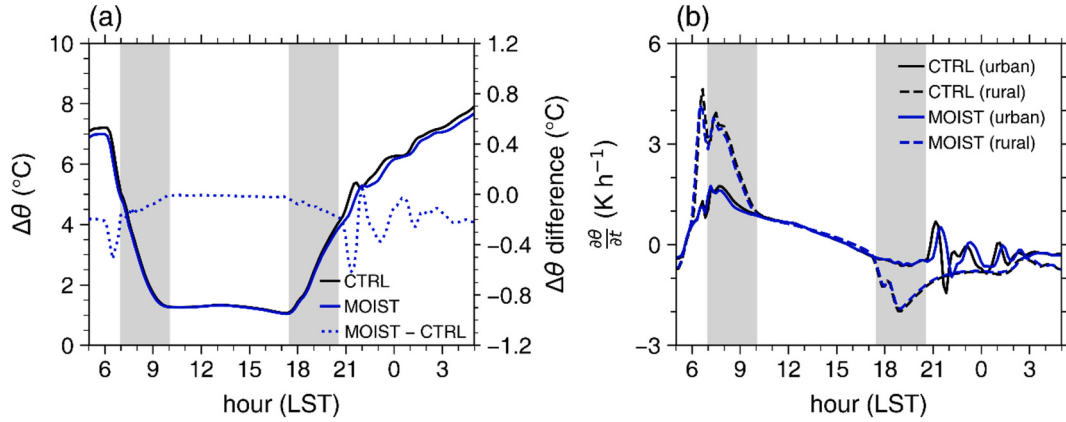


Fig. 11. (a) Diurnal variations of urban (solid) and rural (dashed) potential temperature tendencies in the lowest model layer in the CTRL (black) and MOIST (blue) experiments. (b) Diurnal variations of the urban-rural differences in potential temperature in the lowest model layer in the CTRL (black) and MOIST (blue) experiments. The blue dotted line indicates the difference between the two experiments (MOIST minus CTRL). The shaded areas indicate 0700–1000 LST and 1730–2030 LST. (For interpretation of the references to colour in this figure legend, the reader is referred to the web version of this article.)

than in the CTRL experiment (Fig. 12a). This shows that the radiative heating of air increases and the radiative cooling of air decreases as the background humidity increases. Meanwhile, in both urban and rural areas, the positive $(\partial\theta/\partial t)_{PBL}$ is generally weaker and the negative $(\partial\theta/\partial t)_{PBL}$ is generally stronger in the MOIST experiment than in the CTRL experiment (Fig. 12b). This is attributed to that the turbulent mixing overall increases with increasing background humidity (Fig. C4 in Appendix C). The urban $(\partial\theta/\partial t)_{ADV}$ is generally weaker in the MOIST experiment than in the CTRL experiment, while the rural $(\partial\theta/\partial t)_{ADV}$ exhibits minor differences between the CTRL and MOIST experiments (Fig. 12c).

The mean differences in rural $(\partial\theta/\partial t)_{RAD}$, $(\partial\theta/\partial t)_{PBL}$, and $(\partial\theta/\partial t)_{ADV}$ between the CTRL and MOIST experiments (MOIST minus CTRL) during 0700–1000 LST are $0.06 K h^{-1}$, $-0.19 K h^{-1}$, and $-0.02 K h^{-1}$, respectively (Fig. 12 and Fig. C3 in Appendix C). This

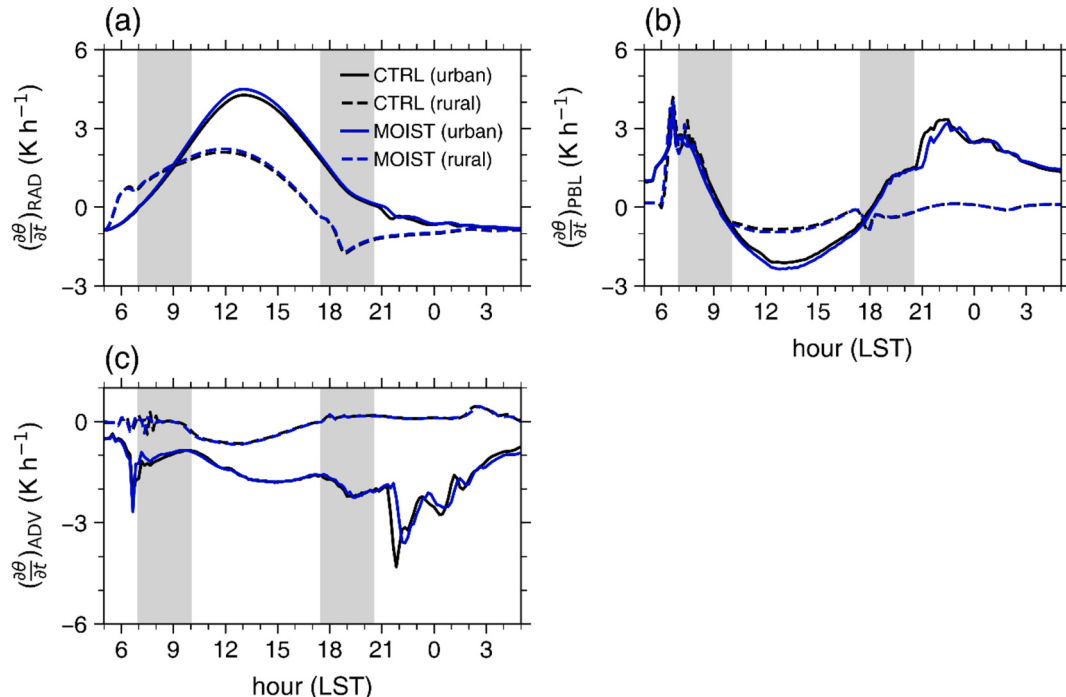


Fig. 12. Diurnal variations of urban (solid) and rural (dashed) potential temperature tendencies in the lowest model layer due to (a) radiative processes, (b) planetary boundary layer processes, and (c) advection in the CTRL (black) and MOIST (blue) experiments. The shaded areas indicate 0700–1000 LST and 1730–2030 LST. (For interpretation of the references to colour in this figure legend, the reader is referred to the web version of this article.)

suggests that the prominently weakened rise in rural 2-m temperature during 0700–1000 LST with increasing background humidity (Fig. 8a) is primarily attributed to the increase in rural turbulent mixing with increasing background humidity. The mean difference in urban $(\partial\theta/\partial t)_{PBL}$ between the CTRL and MOIST experiments during 0700–1000 LST is -0.27 K h^{-1} (Fig. 12b and Fig. C3b in Appendix C) and is offset by the positive mean differences in urban $(\partial\theta/\partial t)_{RAD}$ and $(\partial\theta/\partial t)_{ADV}$ of 0.10 K h^{-1} and 0.11 K h^{-1} , respectively (Fig. 12a and c and Fig. C3a and c in Appendix C). This is responsible for the less weakened rise in urban 2-m temperature during 0700–1000 LST with increasing background humidity (Fig. 8a).

During 1730–2030 LST, the mean differences in rural $(\partial\theta/\partial t)_{RAD}$, $(\partial\theta/\partial t)_{PBL}$, and $(\partial\theta/\partial t)_{ADV}$ between the CTRL and MOIST experiments are 0.05 K h^{-1} , 0.03 K h^{-1} , and -0.01 K h^{-1} , respectively (Fig. 12 and Fig. C3 in Appendix C). This suggests that the prominently weakened decline in rural 2-m temperature during 1730–2030 LST with increasing background humidity (Fig. 8a), which leads to the decrease in nighttime UHI intensity, is primarily attributed to the decrease in the radiative cooling of rural air. The mean differences in urban $(\partial\theta/\partial t)_{RAD}$ and $(\partial\theta/\partial t)_{ADV}$ between the CTRL and MOIST experiments during 1730–2030 LST are, respectively, 0.08 K h^{-1} and 0.03 K h^{-1} (Fig. 12a and c and Fig. C3a and c in Appendix C) and are offset by the negative mean difference in urban $(\partial\theta/\partial t)_{PBL}$ of -0.10 K h^{-1} (Fig. 12b and Fig. C3b in Appendix C). This is responsible for the less weakened decline in urban 2-m temperature during 1730–2030 LST with increasing background humidity (Fig. 8a).

Oleson et al. (2011) showed that the decrease in nighttime UHI intensity with enhanced greenhouse effect is associated with the larger heat storing capacity of urban surface than that of rural surface. On the other hand, the results of this study show that the magnitudes of urban and rural storage heat fluxes during the nighttime do not increase with increasing background humidity (Fig. 9e) and the different changes in near-surface thermodynamic processes between the urban and rural areas are important for changes in UHI intensity with background humidity. This implies that changes in near-surface thermodynamic processes could be important for changes in UHI intensity under climate change.

4. Summary and conclusions

In this study, changes in UHI intensity with background temperature and humidity and their associations with physical processes are examined through idealized ensemble simulations. The daytime and nighttime UHI intensities increase with increasing background temperature and decrease with increasing background humidity. The nighttime UHI intensity exhibits much more prominent changes with background temperature and humidity than the daytime UHI intensity. The increase in UHI intensity with increasing background temperature and the decrease in UHI intensity with increasing background humidity are associated with changes in near-surface thermodynamic processes. As the background temperature increases, in the evening, the radiative cooling of rural air increases and thus the decline in rural 2-m temperature is enhanced. The radiative heating of urban air also decreases, and the urban advective cooling increases. However, the urban turbulent mixing decreases, causing the decline in urban 2-m temperature in the evening to be less enhanced. These are responsible for the increase in nighttime UHI intensity with increasing background temperature. As the background humidity increases, in the evening, the radiative cooling of rural air decreases and thus the decline in rural 2-m temperature is weakened. The radiative heating of urban air also increases, and the urban advective cooling decreases. However, the urban turbulent mixing increases, causing the decline in urban 2-m temperature in the evening to be less weakened. These are responsible for the decrease in nighttime UHI intensity with increasing background humidity.

This study shows that analyzing near-surface thermodynamic processes helps to better understand changes in UHI intensity with background temperature and humidity. This analysis is expected to provide further insights in understanding changes in UHI intensity under heat waves and climate change.

CRediT authorship contribution statement

Kyeongjoo Park: Writing – review & editing, Writing – original draft, Visualization, Validation, Methodology, Investigation, Formal analysis, Data curation. **Jong-Jin Baik:** Writing – review & editing, Supervision, Methodology, Formal analysis, Conceptualization. **Han-Gyul Jin:** Writing – review & editing, Methodology, Formal analysis. **Abeda Tabassum:** Writing – review & editing, Data curation.

Declaration of competing interest

The authors declare that they have no known competing financial interests or personal relationships that could have appeared to influence the work reported in this paper.

Acknowledgements

The authors would like to express their gratitude to two anonymous reviewers for providing valuable comments on this work. This work was supported by the National Research Foundation of Korea (NRF) under grant 2021R1A2C1007044. Han-Gyul Jin was supported by Global Learning & Academic research institution for Master's-PhD students, and Postdocs (LAMP) Program of the National Research Foundation of Korea (NRF) grant funded by the Ministry of Education (No. RS-2023-00301938).

Appendix A. Additional simulations with a scale-aware PBL scheme

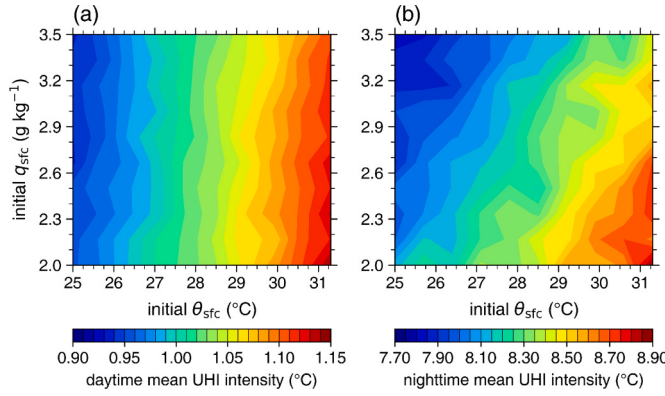


Fig. A1. Same as Fig. 2 except for the simulations with the Shin-Hong scale-aware PBL scheme.

Appendix B. Additional simulations with an initial background wind

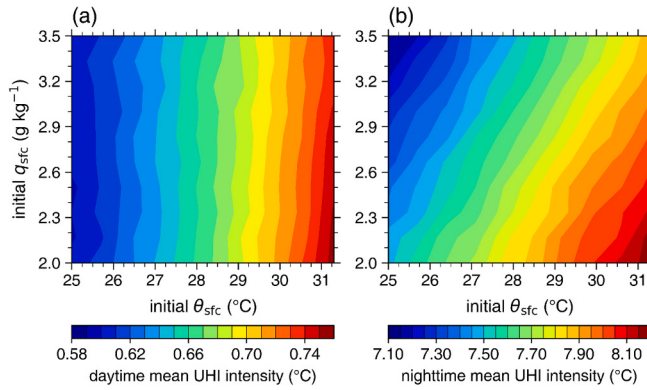


Fig. B1. Same as Fig. 2 except for the simulations in which the initial background wind speed is 5 m s^{-1} .

Appendix C. Differences in urban and rural near-surface thermodynamic processes between experiments

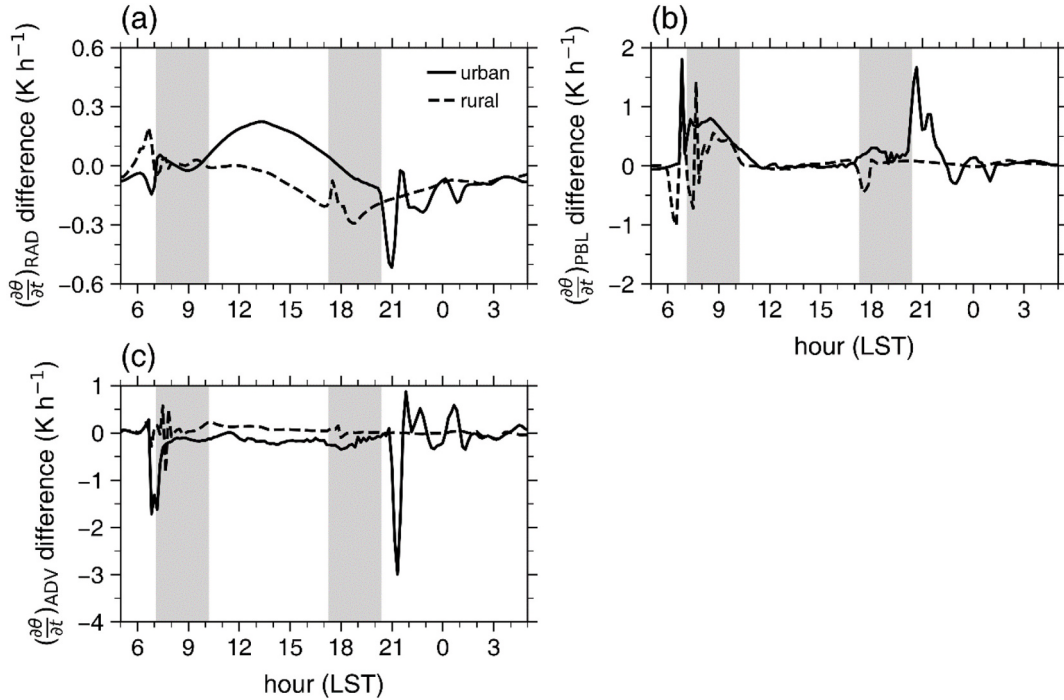


Fig. C1. Diurnal variations of the differences in urban (solid) and rural (dashed) potential temperature tendencies in the lowest model layer due to (a) radiative processes, (b) planetary boundary layer processes, and (c) advection between the CTRL and WARM experiments (WARM minus CTRL). The shaded areas indicate 0710–1010 LST and 1720–2020 LST.

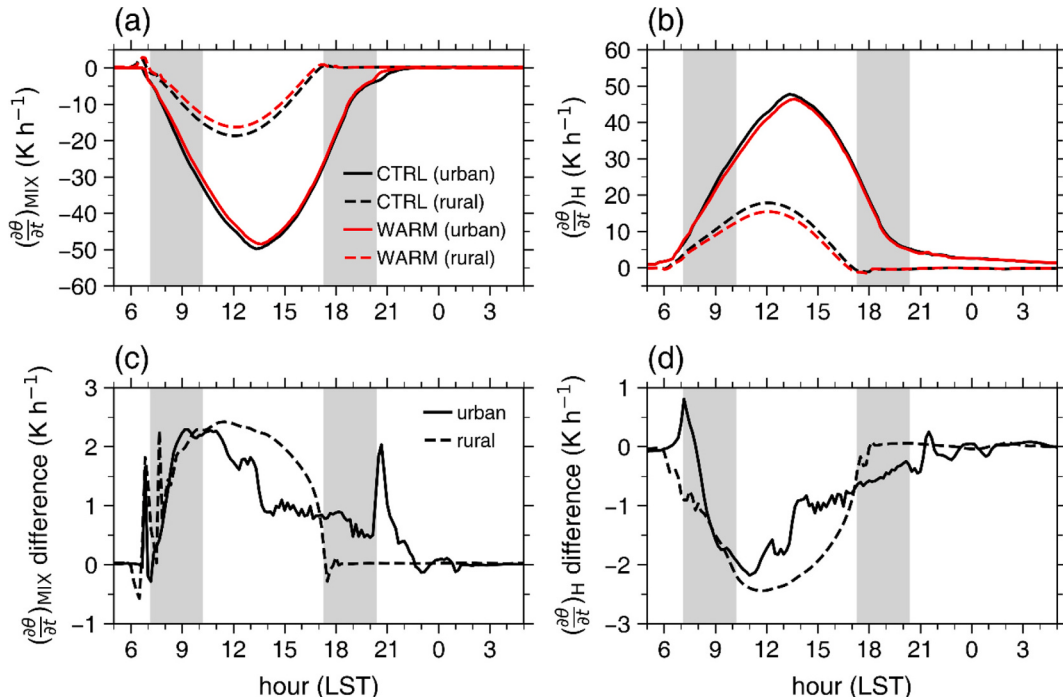


Fig. C2. Diurnal variations of urban (solid) and rural (dashed) potential temperature tendencies in the lowest model layer due to the (a) turbulent mixing and (b) surface sensible heat flux in the CTRL (black) and WARM (red) experiments. Diurnal variations of the differences in urban (solid) and rural (dashed) potential temperature tendencies in the lowest model layer due to the (c) turbulent mixing and (d) surface sensible heat flux between

the CTRL and WARM experiments (WARM minus CTRL). The shaded areas indicate 0710–1010 LST and 1720–2020 LST. (For interpretation of the references to colour in this figure legend, the reader is referred to the web version of this article.)

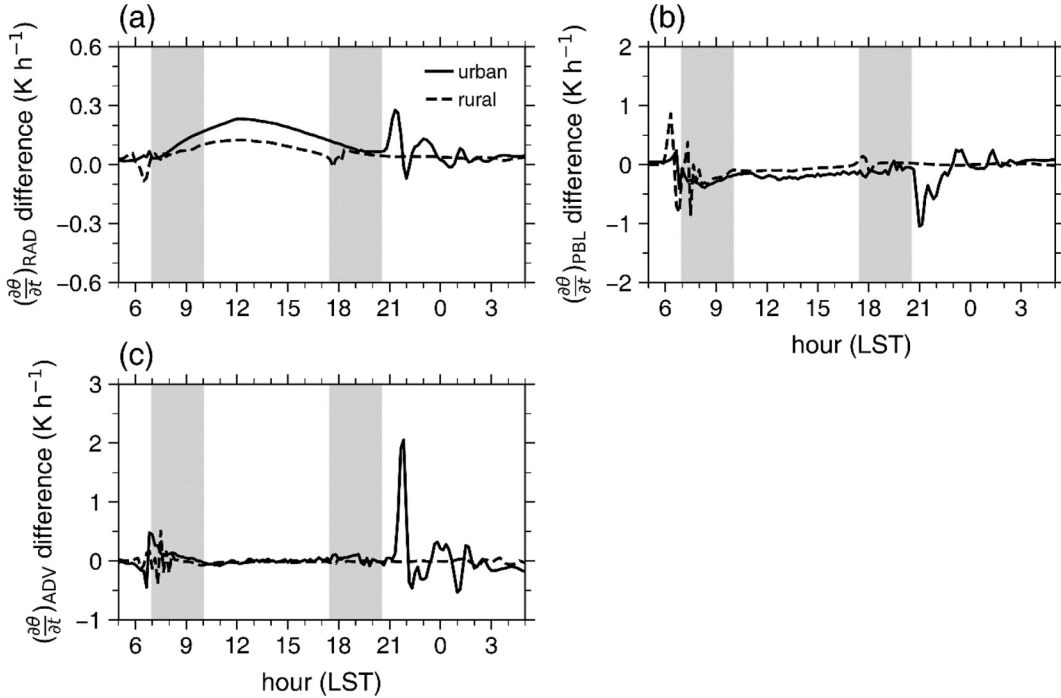


Fig. C3. Diurnal variations of the differences in urban (solid) and rural (dashed) potential temperature tendencies in the lowest model layer due to (a) radiative processes, (b) planetary boundary layer processes, and (c) advection between the CTRL and MOIST experiments (MOIST minus CTRL). The shaded areas indicate 0700–1000 LST and 1730–2030 LST.

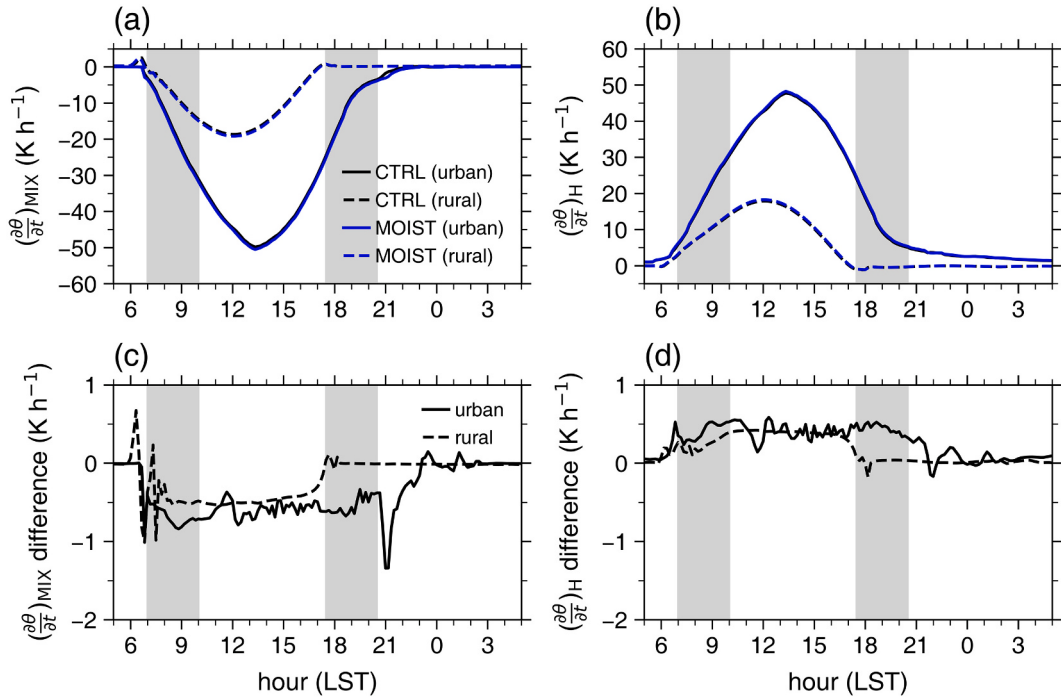


Fig. C4. Diurnal variations of urban (solid) and rural (dashed) potential temperature tendencies in the lowest model layer due to the (a) turbulent mixing and (b) surface sensible heat flux in the CTRL (black) and MOIST (blue) experiments. Diurnal variations of the differences in urban (solid) and rural (dashed) potential temperature tendencies in the lowest model layer due to the (c) turbulent mixing and (d) surface sensible heat flux

between the CTRL and MOIST experiments (MOIST minus CTRL). The shaded areas indicate 0700–1000 LST and 1730–2030 LST. (For interpretation of the references to colour in this figure legend, the reader is referred to the web version of this article.)

Data availability

Data will be made available on request.

References

- Aadhar, S., Mishra, V., 2023. The 2022 mega heatwave in South Asia in the observed and projected future climate. *Environ. Res. Lett.* 18, 104011.
- Ao, X., Wang, L., Zhi, X., Gu, W., Yang, H., Li, D., 2019. Observed synergies between urban heat islands and heat waves and their controlling factors in Shanghai, China. *J. Appl. Meteorol. Climatol.* 58, 1955–1972.
- Arndt, D., Böhner, J., Bechtel, B., 2017. Spatio-temporal variance and meteorological drivers of the urban heat island in a European city. *Theor. Appl. Climatol.* 128, 43–61.
- Basara, J.B., Hall Jr., P.K., Schroeder, A.J., Illston, B.G., Nemunaitis, K.L., 2008. Diurnal cycle of the Oklahoma City urban heat island. *J. Geophys. Res. Atmos.* 113, D20109.
- Chapman, S., Thatcher, M., Salazar, A., Watson, J.E.M., McAlpine, C.A., 2019. The impact of climate change and urban growth on urban climate and heat stress in a subtropical city. *Int. J. Climatol.* 39, 3013–3030.
- Chen, F., Dudhia, J., 2001. Coupling an advanced land surface–hydrology model with the Penn State–NCAR MM5 modeling system. Part I: model implementation and sensitivity. *Mon. Weather Rev.* 129, 569–585.
- Chen, F., Kusaka, H., Bornstein, R., Ching, J., Grimmond, C.S.B., Grossman-Clarke, S., Loridan, T., Manning, K.W., Martilli, A., Miao, S., Sailor, D., Salamanca, F.P., Taha, H., Tewari, M., Wang, X., Wyszogrodzki, A.A., Zhang, C., 2011. The integrated WRF/urban modelling system: development, evaluation, and applications to urban environmental problems. *Int. J. Climatol.* 31, 273–288.
- Cleugh, H.A., Oke, T.R., 1986. Suburban-rural energy balance comparisons in summer for Vancouver, B.C. *Bound.-Layer Meteorol.* 36, 351–369.
- Cui, F., Hamdi, R., Kuang, W., Yang, T., He, H., Termonia, P., De Maeyer, P., 2023. Interactions between the summer urban heat islands and heat waves in Beijing during 2000–2018. *Atmos. Res.* 291, 106813.
- Dudhia, J., 1989. Numerical study of convection observed during the Winter Monsoon Experiment using a mesoscale two-dimensional model. *J. Atmos. Sci.* 46, 3077–3107.
- Fischer, E.M., Oleson, K.W., Lawrence, D.M., 2012. Contrasting urban and rural heat stress responses to climate change. *Geophys. Res. Lett.* 39, L03705.
- Gao, Z., Hou, Y., Chen, W., 2019. Enhanced sensitivity of the urban heat island effect to summer temperatures induced by urban expansion. *Environ. Res. Lett.* 14, 094005.
- Grimmond, C.S.B., Blackett, M., Best, M.J., Barlow, J., Baik, J.-J., Belcher, S.E., Bohnenstengel, S.I., Calmet, I., Chen, F., Dandou, A., Fortuniak, K., Gouvea, M.L., Hamdi, R., Hendry, M., Kawai, T., Kawamoto, Y., Kondo, H., Krayenhoff, E.S., Lee, S.-H., Loridan, T., Martilli, A., Masson, V., Miao, S., Oleson, K., Pigeon, G., Porson, A., Ryu, Y.-H., Salamanca, F., Shashua-Bar, L., Steeneveld, G.-J., Tombrou, M., Voogt, J., Young, D., Zhang, N., 2010. The international urban energy balance models comparison project: first results from phase 1. *J. Appl. Meteorol. Climatol.* 49, 1268–1292.
- Grimmond, C.S.B., Blackett, M., Best, M.J., Baik, J.-J., Belcher, S.E., Beringer, J., Bohnenstengel, S.I., Calmet, I., Chen, F., Coutts, A., Dandou, A., Fortuniak, K., Gouvea, M.L., Hamdi, R., Hendry, M., Kanda, M., Kawai, T., Kawamoto, Y., Kondo, H., Krayenhoff, E.S., Lee, S.-H., Loridan, T., Martilli, A., Masson, V., Miao, S., Oleson, K., Ooka, R., Pigeon, G., Porson, A., Ryu, Y.-H., Salamanca, F., Steeneveld, G.J., Tombrou, M., Voogt, J.A., Young, D.T., Zhang, N., 2011. Initial results from Phase 2 of the international urban energy balance model comparison. *Int. J. Climatol.* 31, 244–272.
- He, X., Wang, J., Feng, J., Yan, Z., Miao, S., Zhang, Y., Xia, J., 2020. Observational and modeling study of interactions between urban heat island and heatwave in Beijing. *J. Clean. Prod.* 247, 119169.
- Hoffmann, P., Krueger, O., Schlünzen, K.H., 2012. A statistical model for the urban heat island and its application to a climate change scenario. *Int. J. Climatol.* 32, 1238–1248.
- Holmes, C.R., Woollings, T., Hawkins, E., de Vries, H., 2016. Robust future changes in temperature variability under greenhouse gas forcing and the relationship with thermal advection. *J. Clim.* 29, 2221–2236.
- Hong, S.-Y., Lim, J.-O.J., 2006. The WRF single-moment 6-class microphysics scheme (WSM6). *J. Korean Meteorol. Soc.* 42, 129–151.
- Hong, S.-Y., Noh, Y., Dudhia, J., 2006. A new vertical diffusion package with an explicit treatment of entrainment processes. *Mon. Weather Rev.* 134, 2318–2341.
- Hu, Y., Hou, M., Jia, G., Zhao, C., Zhen, X., Xu, Y., 2019. Comparison of surface and canopy urban heat islands within megacities of eastern China. *ISPRS J. Photogramm. Remote Sens.* 156, 160–168.
- Inamdar, A.K., Ramanathan, V., 1998. Tropical and global scale interactions among water vapor, atmospheric greenhouse effect, and surface temperature. *J. Geophys. Res. Atmos.* 103, 32177–32214.
- Jiang, S., Lee, X., Wang, J., Wang, K., 2019. Amplified urban heat islands during heat wave periods. *J. Geophys. Res. Atmos.* 124, 7797–7812.
- Jiménez, P.A., Dudhia, J., González-Rouco, J.F., Navarro, J., Montávez, J.P., García-Bustamante, E., 2012. A revised scheme for the WRF surface layer formulation. *Mon. Weather Rev.* 140, 898–918.
- Katzfey, J., Schlünzen, H., Hoffmann, P., Thatcher, M., 2020. How an urban parameterization affects a high-resolution global climate simulation. *Q. J. R. Meteorol. Soc.* 146, 3808–3829.
- Kim, D.W., Lee, S., Clark, J.P., Feldstein, S.B., 2024. Benchmark thermodynamic contributors to the growth and decay of the regional extreme surface temperature. *J. Clim.* 37, 2347–2359.
- Lauwaet, D., De Ridder, K., Saeed, S., Brisson, S., Chatterjee, F., van Lipzig, N.P.M., Maiheu, B., Hooyberghs, H., 2016. Assessing the current and future urban heat island of Brussels. *Urban Clim.* 15, 1–15.
- Li, D., Bou-Zeid, E., 2013. Synergistic interactions between urban heat islands and heat waves: the impact in cities is larger than the sum of its parts. *J. Appl. Meteorol. Climatol.* 52, 2051–2064.
- Li, D., Bou-Zeid, E., 2014. Quality and sensitivity of high-resolution numerical simulation of urban heat islands. *Environ. Res. Lett.* 9, 055001.
- Li, D., Bou-Zeid, E., Oppenheimer, M., 2014. The effectiveness of cool and green roofs as urban heat island mitigation strategies. *Environ. Res. Lett.* 9, 055002.
- Li, D., Sun, T., Liu, M., Yang, L., Wang, L., Gao, Z., 2015. Contrasting responses of urban and rural surface energy budgets to heat waves explain synergies between urban heat islands and heat waves. *Environ. Res. Lett.* 10, 054009.
- Lipson, M.J., Grimmond, S., Best, M., Abramowitz, G., Coutts, A., Tapper, N., Baik, J.-J., Beyers, M., Blunn, L., Boussetta, S., Bou-Zeid, E., De Kauwe, M.G., de Munck, C., Demuzere, M., Fatichi, S., Fortuniak, K., Han, B.-S., Hendry, M.A., Kikegawa, Y., Kondo, H., Lee, D.-I., Lee, S.-H., Lemonsu, A., Machado, T., Manoli, G., Martilli, A., Masson, V., McNorton, J., Meili, N., Meyer, D., Nice, K.A., Oleson, K.W., Park, S.-B., Roth, M., Schoetter, R., Simón-Moral, A., Steeneveld, G.-J., Sun, T., Takane, Y., Thatcher, M., Tsirringakis, A., Varentsov, M., Wang, C., Wang, Z.-H., Pitman, A.J., 2024. Evaluation of 30 urban land surface models in the Urban-PLUMBER project: phase 1 results. *Q. J. R. Meteorol. Soc.* 150, 126–169.
- Liu, Y., Li, Q., Yang, L., Mu, K., Zhang, M., Liu, J., 2020. Urban heat island effects of various urban morphologies under regional climate conditions. *Sci. Total Environ.* 743, 140589.

- Loridan, T., Lindberg, F., Jorba, O., Kotthaus, S., Grossman-Clarke, S., Grimmond, C.S.B., 2013. High resolution simulation of the variability of surface energy balance fluxes across central London with Urban Zones for energy partitioning. *Bound.-Layer Meteorol.* 147, 493–523.
- Ma, X., Miao, S., Masson, V., Wurtz, J., Zhang, Y., Wang, J., Huang, X.-Y., Yan, C., 2024. The synergistic effects of urbanization and an extreme heatwave event on urban thermal environment in Paris. *Urban Clim.* 53, 101785.
- Mitchell, J.F.B., 1989. The “Greenhouse” effect and climate change. *Rev. Geophys.* 27, 115–139.
- Mlawer, E.J., Taubman, S.J., Brown, P.D., Iacono, M.J., Clough, S.A., 1997. Radiative transfer for inhomogeneous atmospheres: RRTM, a validated correlated-k model for the longwave. *J. Geophys. Res. Atmos.* 102, 16663–16682.
- Obregón, M.A., Costa, M.J., Silva, A.M., Serrano, A., 2018. Impact of aerosol and water vapour on SW radiation at the surface: sensitivity study and applications. *Atmos. Res.* 213, 252–263.
- Oke, T.R., 1982. The energetic basis of the urban heat island. *Q. J. R. Meteorol. Soc.* 108, 1–24.
- Oke, T.R., Mills, G., Christen, A., Voogt, J.A., 2017. *Urban Climates*. Cambridge University Press.
- Oleson, K.W., Bonan, G.B., Feddema, J., Jackson, T., 2011. An examination of urban heat island characteristics in a global climate model. *Int. J. Climatol.* 31, 1848–1865.
- Park, K., Jin, H.-G., Baik, J.-J., 2023. Contrasting interactions between urban heat islands and heat waves in Seoul, South Korea, and their associations with synoptic patterns. *Urban Clim.* 49, 101524.
- Peng, S., Feng, Z., Liao, H., Huang, B., Peng, S., Zhou, T., 2019. Spatial-temporal pattern of, and driving forces for, urban heat island in China. *Ecol. Indic.* 96, 127–132.
- Perkins, S.E., Alexander, L.V., Nairn, J.R., 2012. Increasing frequency, intensity, and duration of observed global heatwaves and warm spells. *Geophys. Res. Lett.* 39, L20714.
- Philippon, R., Dürr, B., Ohmura, A., Ruckstuhl, C., 2005. Anthropogenic greenhouse forcing and strong water vapor feedback increase temperature in Europe. *Geophys. Res. Lett.* 32, L19809.
- Pigeon, G., Lemonsu, A., Grimmond, C.S.B., Durand, P., Thouron, O., Masson, V., 2007. Divergence of turbulent fluxes in the surface layer: case of a coastal city. *Bound.-Layer Meteorol.* 124, 269–290.
- Possega, M., Aragão, L., Ruggieri, P., Santo, M.A., Di Sabatino, S., 2022. Observational evidence of intensified nocturnal urban heat island during heatwaves in European cities. *Environ. Res. Lett.* 17, 124013.
- Qian, Y., Chakraborty, T.C., Li, J., Li, D., He, C., Sarangi, C., Chen, F., Yang, X., Leung, L.R., 2022. Urbanization impact on regional climate and extreme weather: current understanding, uncertainties, and future research directions. *Adv. Atmos. Sci.* 39, 819–860.
- Ramamurthy, P., González, J., Ortiz, L., Arend, M., Moshary, F., 2017. Impact of heatwave on a megacity: an observational analysis of New York City during July 2016. *Environ. Res. Lett.* 12, 054011.
- Ren, S., Stroud, C.A., 2020. Temperature response from the change of surface heat flux and vertical diffusivity by urbanization. *Atmosphere* 11, 978.
- Ryu, Y.-H., Baik, J.-J., 2012. Quantitative analysis of factors contributing to urban heat island intensity. *J. Appl. Meteorol. Climatol.* 51, 842–854.
- Ryu, Y.-H., Baik, J.-J., Lee, S.-H., 2011. A new single-layer urban canopy model for use in mesoscale atmospheric models. *J. Appl. Meteorol. Climatol.* 50, 1773–1794.
- Sachindra, D.A., Ng, A.W.M., Muthukumaran, S., Perera, B.J.C., 2016. Impact of climate change on urban heat island effect and extreme temperatures: a case-study. *Q. J. R. Meteorol. Soc.* 142, 172–186.
- Salamalikis, V., Vamvakas, I., Guemard, C.A., Kazantzidis, A., 2021. Atmospheric water vapor radiative effects on shortwave radiation under clear skies: a global spatiotemporal analysis. *Atmos. Res.* 251, 105418.
- Sánchez, E., Yagüe, C., Gaertner, M.A., 2007. Planetary boundary layer energetics simulated from a regional climate model over Europe for present climate and climate change conditions. *Geophys. Res. Lett.* 34, L01709.
- Sarangi, C., Qian, Y., Li, J., Leung, L.R., Chakraborty, T.C., Liu, Y., 2021. Urbanization amplifies nighttime heat stress on warmer days over the US. *Geophys. Res. Lett.* 48 e2021GL095678.
- Schatz, J., Kucharik, C.J., 2014. Seasonality of the urban heat island effect in Madison, Wisconsin. *J. Appl. Meteorol. Climatol.* 53, 2371–2386.
- Scott, A.A., Waugh, D.W., Zaitchik, B.F., 2018. Reduced Urban Heat Island intensity under warmer conditions. *Environ. Res. Lett.* 13, 064003.
- Sherwood, S.C., Huber, M., 2010. An adaptability limit to climate change due to heat stress. *Proc. Natl. Acad. Sci. U. S. A.* 107, 9552–9555.
- Shin, H.H., Hong, S.-Y., 2015. Representation of the subgrid-scale turbulent transport in convective boundary layers at gray-zone resolutions. *Mon. Weather Rev.* 143, 250–271.
- Skamarock, W.C., Klemp, J.B., Dudhia, J., Gill, D.O., Liu, Z., Berner, J., Wang, W., Powers, J.G., Duda, M.G., Barker, D.M., Huang, X.-Y., 2019. A description of the Advanced Research WRF model version 4. NCAR Tech. Note TN-556+STR.
- Sun, T., Grimmond, C.S.B., Ni, G.-H., 2016. How do green roofs mitigate urban thermal stress under heat waves? *J. Geophys. Res. Atmos.* 121, 5320–5335.
- Swinbank, W.C., 1963. Long-wave radiations from clear skies. *Q. J. R. Meteorol. Soc.* 89, 339–348.
- Türkş, M., Sümer, U.M., 2004. Spatial and temporal patterns of trends and variability in diurnal temperature ranges of Turkey. *Theor. Appl. Climatol.* 77, 195–227.
- Wang, K., Ye, H., Chen, F., Xiong, Y., Wang, C., 2012. Urbanization effect on the diurnal temperature range: different roles under solar dimming and brightening. *J. Clim.* 25, 1022–1027.
- Wang, L., Li, D., Zhang, N., Sun, J., Guo, W., 2020. Surface urban heat and cool islands and their drivers: an observational study in Nanjing, China. *J. Appl. Meteorol. Climatol.* 59, 1987–2000.
- White, R.H., Anderson, S., Booth, J.F., Braich, G., Draeger, C., Fei, C., Harley, C.D.G., Henderson, S.B., Jakob, M., Lau, C.-A., Admasu, L.M., Narinesingh, V., Rodell, C., Roocroft, E., Weinberger, K.R., West, G., 2023. The unprecedented Pacific Northwest heatwave of June 2021. *Nat. Commun.* 14, 727.
- Willett, K.M., Sherwood, S., 2012. Exceedance of heat index thresholds for 15 regions under a warming climate using the wet-bulb globe temperature. *Int. J. Climatol.* 32, 161–177.
- Zaitchik, B.F., Macalady, A.K., Bonneau, L.R., Smith, R.B., 2006. Europe's 2003 heat wave: a satellite view of impacts and land-atmosphere feedbacks. *Int. J. Climatol.* 26, 743–769.
- Zhao, L., Oppenheimer, M., Zhu, Q., Baldwin, J.W., Ebi, K.L., Bou-Zeid, E., Guan, K., Liu, X., 2018. Interactions between urban heat islands and heat waves. *Environ. Res. Lett.* 13, 034003.
- Zhou, K., Zhong, L., Wang, Z., Liu, J., Wu, Z., 2024. Evaluating the impacts of land use/land cover changes and climate variations on urban heat islands using the WRF-UCM model in Hefei, China. *Clim. Change* 177, 121.
- Zong, L., Liu, S., Yang, Y., Ren, G., Yu, M., Zhang, Y., Li, Y., 2021. Synergistic influence of local climate zones and wind speeds on the urban heat island and heat waves in the megacity of Beijing, China. *Front. Earth Sci.* 9, 673786.
- Zou, Z., Yan, C., Yu, L., Jiang, X., Ding, J., Qin, L., Wang, B., Qiu, G., 2021. Impacts of land use/ land cover types on interactions between urban heat island effects and heat waves. *Build. Environ.* 204, 108138.